

A SYNOPTIC-SCALE ENVIRONMENT ASSOCIATED WITH SIGNIFICANT NOCTURNAL TORNADO EVENTS IN THE GREAT PLAINS

Corey M. Mead* and Richard L. Thompson
NOAA/NWS/Storm Prediction Center, Norman, Oklahoma

1. INTRODUCTION

Past climatological studies (e.g. Concannon et al. 2000 and Brooks et al. 2003) have clearly defined a spatial maximum in tornado occurrence over the Great Plains, extending from western Texas into eastern Colorado, Nebraska and Iowa. The general location of this maximum is annually repeatable and largely dependent on the underlying geography of the region. To the south, the Gulf of Mexico provides a source of moist air in the low levels, whereas the high terrain of the western U.S. and northern Mexico serve as a genesis region for the development of an elevated mixed layer (EML, Carlson et al. 1983 and Lanicci and Warner 1991) that can contribute to the superposition of high lapse rates over near-surface moisture, yielding a vertical thermal stratification resembling a Type 1 or “loaded gun” sounding profile as defined by Miller (1972).

The characteristics of this Great Plains environment are largely responsible for the strong diurnal signal in tornado occurrence (Kelly et al. 1978) whereby the cap associated with the EML often delays the thunderstorm development and subsequent severe weather to near or just after the peak of diurnal heating. Thereafter, the relatively rapid development of convective inhibition (CIN, Colby 1984) can occur as the boundary layer underlying the EML begins to stabilize and decouple. This typically leads to the dissipation of ongoing, diurnally-initiated storms, while limiting the potential for subsequent, surface-based thunderstorm initiation.

The late afternoon to early evening peak in tornado frequency, coupled with low population density and the lack of forests (i.e. greater visibility) all contribute to a reduced vulnerability to fatalities over the central U.S. when compared to other parts of the country east of the Rocky Mountains (Ashley 2007). However, when nighttime tornadoes do

occur in the Plains, they can create significant challenges for the integrated warning system (Doswell et al. 1999) and pose a threat to life and property. Recent examples include: 1) the 21 April 2001 Hoisington, KS tornado, which resulted in one fatality, 28 injuries, and \$43 million in damages (*Storm Data* 2001). And, 2) the 4 May 2007 tornado, which leveled the rural community of Greensburg, KS, causing 11 fatalities, 63 injuries, and \$250 million in property damage (*Storm Data* 2007).

The primary motivation of this work stems, in part, from these two events, which are associated with a specific, reoccurring synoptic pattern that can foster an enhanced threat for significant, late evening and/or nighttime tornadoes in the Great Plains. The authors' identification of this pattern and initial attempts to apply an anecdotally-constructed conceptual model to operational forecasts dates back to 2002. Since then, a number of these events have been anticipated successfully. However, the general tendency has been to underforecast the number and intensity of tornadoes in several of the “higher end” events. In other cases, the pattern was identified and tornadoes were forecast, but none were observed.

To address these shortcomings, we endeavor first to provide a detailed description of the identified synoptic pattern, which from a broad perspective, is nearly identical for both significantly tornadic (hereafter sigtor) and non-tornadic (hereafter nontor) severe weather events. Second, we will highlight the importance of low-level jet (LLJ) formation, describing how this feature can condition the environment for the development and/or sustenance of violent, deep moist convection after dark. Finally, given the similarities in the large-scale pattern for the sigtor and nontor cases, we show through the use of 0-hr RUC-2 analysis soundings (Thompson et al. 2003; hereafter T03) that the characteristics of the lower-tropospheric thermal and

* Corresponding author address: Corey M. Mead,
NOAA Storm Prediction Center, National Weather
Center, 120 David L. Boren Blvd, Norman, OK 73072.
Email: Corey.Mead@noaa.gov

moisture profile can be used to discriminate between the two classes of events.

It should be noted that not *all* significant nocturnal tornado occurrences in the Great Plains are associated with this particular synoptic pattern. Recent examples include multiple EF2-EF3 tornadoes over the central and southern High Plains on 28 March 2007 and an EF4 tornado in south-central Oklahoma on 10 February 2009. These cases exhibited a much more dynamic large-scale pattern than that documented by this study.

2. DATA COLLECTION AND METHODOLOGY

The authors' knowledge of several synoptically-similar, nocturnal tornado events in the central and southern Plains (two examples are provided in Figs. 1 and 2) served as the basis for initial data collection for this study. Questions regarding the frequency of this pattern and which attendant processes or components are critical to nighttime tornado production led to an expansion of the dataset. This was accomplished through the use of the National Oceanic and Atmospheric Administration (NOAA) *Storm Data* and "Storm Events" database (available online at <http://www4.ncdc.noaa.gov/cgi-win/wwwcgi.dll?wwEvent~Storms>) and the subjective matching of objectively-analyzed, observed upper-air data to the identified synoptic pattern. A total of 35 cases was identified; 16 sigtor (Table 1), and 19 nontor. The period of analysis was restricted to 1999-2009 owing to decreasing availability of pertinent data prior to this time.

To be considered a sigtor case, the prospective event had to match the identified synoptic pattern with at least one EF2 or greater tornado reported after apparent solar sunset (calculated online at <http://www.esrl.noaa.gov/gmd/grad/solcalc/>). Although some sky light persists after sunset, the average report time for the beginning of the most intense tornado for each case was 105 minutes after sunset. No constraint was placed on the occurrence of a tornado prior to sunset. However, in only one case did the most intense tornado of the entire severe weather episode occur during the daylight hours. A total of 39 significant, nocturnal tornadoes was found for the 16 sigtor cases (Fig. 3).

To determine possible failure modes (i.e. nonoccurrence of nocturnal tornadoes) of this synoptic pattern, a nontor (null) case set was collected through a similar method of positive

pattern matching on the synoptic scale, but without the occurrence of nighttime tornadoes (see Fig. 4 as a case example). All of the identified nontor cases were associated with thunderstorms (including supercells) that produced severe hail and/or damaging winds over the Great Plains within the same convective day (1200 UTC to 1200 UTC). These events included a combination of diurnally-driven storms that dissipated near or just after sunset, diurnal storms that persisted into the night, or nocturnal storms that lasted through a portion of the night. Weak tornadoes (one EF-1 and two EF-0s) were reported in two of the cases. However, the report times for these were between three and four hours *prior* to sunset.

A hypothesis being tested in this study is that the LLJ plays a critical role in air mass destabilization and the enhancement of vertical shear during the evening into nighttime hours. And, that specific details in the warm sector air mass along the LLJ axis, namely the thermal and moisture characteristics of the lower troposphere, are of critical importance in discriminating between the sigtor and nontor cases. In order to test this hypothesis, "proximity" in the ambient environment was determined by where the LLJ axis intersected the northern edge of the warm sector air mass at 0300 UTC (using a subjectively-determined, representative dew point value; see Fig. 5).

Traditionally, a proximity environment has been defined through spatial and temporal constraints relative to observed severe storms (see Section 4 for a more detailed background on this topic). However, this study is interested in the environmental changes occurring along the LLJ axis which is hypothesized to be a critical component of this synoptic pattern. Therefore, our criteria were chosen such that the technique can be applied prior to initiation of storms, during the time of LLJ development. As opposed to selecting some arbitrary location within the surface warm sector along the LLJ axis, we believed that the use of the northern edge was more definitive, with this location often delineated by a baroclinic zone which can serve as the focus for storm development. The temporal criterion of 0300 UTC was chosen for two reasons. First, as will be shown in the subsequent section, this synoptic pattern is associated with a rapid acceleration of the LLJ between 0100 and 0300 UTC. Second, this time corresponds well to the average touchdown time of the most intense tornado for each of the sigtor cases (0323 UTC) as documented by *Storm Data*.

The proximity location determined by our method was compared to the touchdown point of the most intense tornado for each of the sigtor cases (not shown). On average, this approach defines a proximity location within about 100 km of the observed tornado occurrence, which is similar to the proximity criteria recommendations by Potvin et al. (2010).

For the purpose of this study, the LLJ was defined as a southerly wind maximum that develops at or below 1500 m AGL that satisfies one or more of the speed criteria established in Bonner (1968). However, this low-level wind maximum did not necessarily represent the greatest speed in the tropospheric wind profile; that is, there may be stronger winds in the middle and upper troposphere similar to the coupling of the low-level and upper-level jet streams as documented by Uccellini and Johnson (1979). The development and evolution of the LLJ in this synoptic setting was documented through the use of plan view and time-height displays of NOAA 404-MHz Profiler Network (NPN) and Weather Surveillance Radar-1988 Doppler (WSR-88D) velocity azimuth display (VAD). These data were used to identify the location and the magnitude of the LLJ on an hourly basis from 0000-0600 UTC for each of the 35 cases.

Once the proximity location was identified for each case, a combination of Rapid Update Cycle-2 (RUC-2) (Benjamin et al. 2002) analysis grids and RUC analysis profiles (Benjamin et al. 2004) were used to construct soundings for the analysis of the sigtor and nontor environments (T03). RUC-2 analysis grids were used from 1999-2003 with the RUC analysis profiles used from 2004-2009. The RUC-2 analysis grids were available at either 20- or 40-km horizontal grid spacing (again based on availability), on isobaric surfaces with 25-hPa vertical resolution (e.g., 1000, 975, 950, 925 hPa, etc.). However, the RUC analysis profiles provide full model resolution in the vertical. Both data types were displayed using the LINUX version of the Skew-T Hodograph Analysis and Research Program (NSHARP; Hart and Korotky 1991) software. RUC-2 analysis grids were also used in the creation of plan view isobaric and sea-level pressure analyses, depicting the synoptic pattern. These analyses were created using the General Meteorology Package (GEMPAK; desJardins 1991).

3. SYNOPTIC PATTERN

3.1 General Overview

One of the major goals of this paper is to document the synoptic pattern in which these nocturnal tornado events occur. A general overview of this pattern is provided in Fig. 6 where mean sea-level pressure and 500-hPa geopotential height fields derived from RUC analysis grids at 0000 UTC are depicted for both the sigtor and nontor cases. In both subsets, a major trough is present over the western United States with prevailing southwesterly midlevel winds downstream over the Great Plains. Slight differences do exist over the eastern United States where, on average, the 500-hPa geopotential height and sea-level pressure fields are higher for the sigtor cases. Whereas an in-depth analysis and discussion of these differences is beyond the scope of this paper, our operational experience suggests that these differences can have notable impacts on low-level trajectories over the Gulf of Mexico basin and the quality of boundary layer moisture return observed over the Great Plains (Thompson et al. 1994).

In many of the documented cases, the western U.S. trough is still in the process of intensifying, with the primary trough axis generally near or west of the Continental Divide. This mid and upper level trough location results in the most substantial mid and upper level forcing for ascent remaining well to the west of the Great Plains at the time of the sigtor events. However, in some of the cases, analyses of water vapor satellite imagery and NPN data reveal the presence of a low amplitude short wave trough or jet streak downstream from the primary trough within the southwesterly flow field over the Central or Southern Rockies. These features are often manifest as cirrus streaks or plumes (Roebber et al. 2002 and Lemon and Umschied 2009) and can enhance lower tropospheric processes such as lee cyclogenesis and LLJ formation.

Another commonly observed mid-level feature is a short wave trough which is in the process of de-amplifying over the north-central United States or south-central Canada. Although not resolved in the mean geopotential height fields in Fig. 6, a good illustration of this weakening, lead short wave trough is provided in Figs. 1a and 2a. It is believed that this weakening, lead system may serve to initiate the poleward transport of low-level moisture from the Gulf of Mexico. Additionally, an associated trailing surface front is often observed to stall over the central or southern Plains which can serve as the focus for storm initiation during these nocturnal episodes.

In the lower troposphere, the development or deepening of a lee cyclone is observed over the High Plains, with a dryline extending southward from this low pressure area into Western Texas. As mentioned above, a common observation is for the western extension of a frontal system associated with the passage of a weakening, lead short wave trough to stall or retreat northward during the latter half of the day in response to the High Plains cyclogenesis. The initiation of the supercells responsible for the significant nocturnal tornadoes typically occurs along the dryline (Fig. 7a) or the previously-mentioned front (Fig. 7b). However, in a few cases, moisture discontinuities or “surges” found within the system warm sector have been observed to provide the focus for storm development (Fig. 7c). These moisture surges can be in the form of retreating dryline segments documented by Hane et al. (2001), Bluestein et al. (1988) and Bluestein et al. (1989), or moisture discontinuities separate from the dryline, often observed as radar finelines in the open warm sector.

Though this synoptic pattern can occur at any time of year, it is most commonly observed in the spring and fall with the months of April and May having the highest number of documented cases (Fig. 8). Although subsynoptic-scale details may vary, the broad configuration of this particular pattern appears to be reproducible as shown in Fig. 9. A composite of the 5700 and 5760 m isohypses or “spaghetti diagram” at 500-hPa for all of the cases clearly indicates the presence of a similarly-phased, synoptic-scale trough over the Intermountain West and prevailing southwesterly flow across the Great Plains. This notion of repeatability is particularly apparent within this southwesterly flow where a rather tight clustering of isohypses (at both 5700 and 5760 meters) is observed from the Southern Rockies into the Central Plains. The pattern then becomes much more variable over the eastern third of the U.S., but as was discussed earlier in this section, there is a tendency for more pronounced ridging in the sigtor cases.

3.2 The Low-level Jet

It is believed that one of the more important processes associated with this pattern is the development of a LLJ around sunset. Initial research on the nocturnal boundary layer wind maximum (NBLWM) focused on the physical processes contributing to its development (e.g. Blackadar 1957, Wexler 1961 and Holton 1967) and climatology (Bonner 1968), largely under quiescent synoptic-scale conditions. In these instances, an

inertial oscillation in the lower troposphere directly contributes to the formation of the NBLWM just above the boundary layer temperature inversion, with the maximum wind speeds typically reached between 0600 and 1200 UTC.

However, other dynamical processes can contribute to LLJ development. Reiter (1969) documented the presence of lower tropospheric wind maxima over the Midwest in conjunction with synoptic or subsynoptic-scale forcing. Hoecker (1963) and Bonner (1966) showed examples where LLJ formation occurred in the presence of lee troughing or cyclogenesis east of the Rocky Mountains. Furthermore, Uccellini and Johnson (1979) and Uccellini (1980) demonstrated how upper-level jet streaks (ULJ) and deepening synoptic systems can contribute to the development of and/or intensification of the LLJ, regardless of time of day. In these cases, a linkage between the ULJ and LLJ occurs through mass-momentum adjustment processes.

Analyses of WPN and WSR-88D VAD data from the 35 cases in this study indicate that the most rapid acceleration in low-level (i.e., 500-1500 m AGL) wind speeds occur in the 0100-0300 UTC timeframe (Fig. 10). Not only are the temporal characteristics of this response similar for both the sigtor and nontor subsets, but so is the spatial evolution as shown in Fig. 11. By 0300 UTC, the spatial distribution of the LLJ is quite similar to that of the observational frequency of occurrence diagram (Fig. 12) developed by Bonner (1965). However, this LLJ evolution is much sooner than what can be accounted for by the inertial oscillation process with the NBLWM alone. This indicates that the dynamical processes, contributing to the deepening surface cyclone, are likely responsible for hastening LLJ development.

An important characteristic of the LLJ is its ability to transport heat and moisture (Means, 1952, 1954, Bonner, 1966) rapidly poleward, contributing to the destabilization of the pre-convective environment. Often times, this convective instability is released owing to increased low-level convergence and associated vertical motion in the exit region of the LLJ (Beebe and Bates 1955; Uccellini 1990). In addition to modifying the thermodynamic characteristics of the local environment, Maddox (1993) illustrated how the development of the nocturnal LLJ can dramatically increase storm-relative helicity (SRH, Lilly 1983, 1986; Davies-Jones 1984, Davies-Jones et al. 1990). Given other favorable environmental

conditions, this increase in near-ground shear promotes supercell development.

Figure 13 is an illustration of how the LLJ can contribute to a large, rapid modification of the local environment. Aside from slight cooling below 850 hPa, little change is observed through the remainder of the temperature profile from 0000 to 0400 UTC. In contrast, the moisture profile exhibits considerable moistening below 300 hPa with perhaps the most notable change occurring below 850 mb where the mean mixed-layer (ML, defined as the lowest 100 hPa) mixing ratio nearly doubles, increasing from 7.9 g kg^{-1} to 14.9 g kg^{-1} . Despite minor cooling of the boundary layer, the marked increase in moisture contributes to a local increase in MLCAPE of over 3000 J kg^{-1} between 0000 and 0400 UTC.

In addition to the large increase in MLCAPE and lowering of lifting condensation level (LCL) and the level of free convection (LFC), the two hodographs reveal the most pronounced increase in wind speeds occurring through the lowest 1-2 km AGL. In fact, 0-1 km vector shear magnitude and 0-1 km SRH increase markedly between 0000 and 0400 UTC, from 6.5 m s^{-1} and $99 \text{ m}^2 \text{ s}^{-2}$ to 16.5 m s^{-1} and $399 \text{ m}^2 \text{ s}^{-2}$, respectively. These rapid environmental changes associated with the development of the LLJ can actually result in an increased threat for tornadic thunderstorms at the time of day when, from a climatological perspective, the threat is typically diminishing.

Recall that the average touchdown time of the most intense tornado for each case was 0323 UTC. Therefore, Fig. 14 likely gives a good approximation of the LLJ magnitude and location during the time of many of these sigtor events. Based on the location of the tornado events relative to the LLJ axis, it is reasonable to assume that the potential enhancements in convective instability and vertical shear in association with the LLJ development (as shown in Fig. 13) are likely playing a role in the formation and sustenance of the documented tornadic storms.

4. RUC SOUNDING ANALYSIS RESULTS

Initial proximity sounding studies were performed by Showalter and Fulks (1943), Fawbush and Miller (1954), and Beebe (1955, 1958) where thermodynamic and kinematic characteristics of the ambient environment were linked to subsequent severe storm evolution. Refinements in this type of

severe storm research occurred through the 1970s (e.g., Maddox 1976; Darkow and McCann 1977) and into the 1990s (Davies and Johns 1993; Johns et al. 1993; Brooks et al. 1994) where assessments of vertical shear and buoyancy in severe storm environments were made using observed sounding data. However, the combination of the rather coarse spatial network and only twice daily launches of these observations severely limits the potential for research studies to accumulate a large sample of proximity soundings within a reasonable amount of time. In fact, Maddox (1976) estimated that several hundred years may be necessary to accumulate a large sample of close proximity soundings for tornadic storms.

In order to accelerate the data collection process and thereby create as large a sample size of observed proximity soundings for severe storms as possible, Rasmussen and Blanchard (1998; hereafter RB98) and Craven et al. (2002a; hereafter C02) used much less stringent time and space criteria to accumulate 6793 and 60,090 soundings, respectively. However, based on analyses of the RB98 supercell classification scheme by T03 and the proximity criteria of 185 km and 3h before and after observed sounding time in C02, under-sampling issues (RB98) and the inability to associate specific classes of severe weather with specific storm types (C02) have limited the utility of this approach.

Consequently, T03 used 40-km RUC-2 analysis grids to create proximity (30 min and within 40 km of a radar identified supercell) soundings to assess local storm environments. Through comparison to observed soundings, they determined that the RUC-2 soundings were reasonably accurate, allowing them to be used as a surrogate for observed soundings in supercell environments. This approach has allowed for a number of relatively large datasets to be compiled such as Davies (2004) – 518 soundings, Thompson et al. (2007, hereafter T07) – 1185 soundings and Davies and Fischer (2009; hereafter DF09) – 1705 soundings.

Since it has been shown that the synoptic-scale characteristics of the sigtor and nontor cases are fairly similar, RUC proximity sounding data have been employed in hopes of making meaningful discrimination between the two subsets. Owing to known cool and dry biases near the ground (T03), the sounding profiles were modified with nearby surface observations, similar to T07.

4.1 Thermodynamic Parameters

Doswell et al. (1996) describe three basic “ingredients” for thunderstorms: lower tropospheric moisture, conditional instability and some lifting mechanism, such as a convergent boundary. Two of these ingredients, lower tropospheric moisture and conditional instability, are often combined into the single parameter Convective Available Potential Energy (CAPE, Monchrief and Miller 1976) for use in assessing the amount of buoyancy in a given environment (see Doswell and Schultz 2006 for a discussion of the advantages and disadvantages of various convective parameters). As recommended by Craven et al. (2002b), the mean temperature and dewpoint in the lowest 100 hPa (ML) were used in all of the thermodynamic calculations, and all CAPE calculations included the virtual temperature correction (Doswell and Rasmussen 1994).

From the box and whisker plot shown in Fig. 15, it is clear that both the sigtor and nontor environments are associated with moderate to strongly unstable environments, but the MLCAPE values for the sigtor events are almost one quartile higher at both 0000 and 0300 UTC. The 0300 UTC median value of 2458 J kg^{-1} for the sigtor subset is in relatively good agreement with the median value of 2654 J kg^{-1} for the Plains nighttime significant tornado subset found in DF09 and the median value of 2152 J kg^{-1} for the significantly tornadic supercells in T03.

One very interesting result is the local *increase* in MLCAPE from 0000 to 0300 UTC for both subsets, which is contrary to the typical diurnal tendency. Time trends in ML mixing ratio (Fig. 16) and 3-6 km AGL lapse rate (see Table 2 for mean values) indicate that this observation is due primarily to increasing boundary layer moisture content, which is consistent with the example provided in Fig. 13.

Of considerable importance in forecasting the development of tornadic storms, especially after dark, is ability to assess the degree of static stability within the boundary layer. This can be done through the use of CIN calculations, which is an integrated area of negative buoyancy below the positive CAPE area on a thermodynamic diagram. The results from RB98, Davies (2004) and DF09 indicate that tornadic storms are typically associated with lower values of CIN than other classes of deep, moist convection. Exceptions do occur where significant tornadoes are observed in near-surface environments featuring rather deep stable layers (Fischer and Davies 2009). In these relatively infrequent cases, a plausible hypothesis advanced

by Fischer and Davies (2009) is that the combination of strong low-level shear and conditional instability allow for the maintenance of supercells with intense mesocyclones (Rotunno and Klemp 1982), such that forced ascent with the mesocyclone overwhelms the ambient CIN and continues to lift storm inflow parcels to their LFCs.

The results of Fig. 17 are consistent with RB98, Davies (2004), DF09 and Fischer and Davies (2009) in that the sigtor cases are associated with notably less MLCIN. In fact, this discrimination increases between 0000 UTC and 0300 UTC, where the 90th percentile CIN value for the sigtor cases is considerably less than the 25th percentile CIN value for the nontor counterparts. This separation is possibly due to the observation that the sigtor cases are typically associated with higher boundary layer moisture content (Fig. 16) which effectively limits the amount of radiational cooling and resultant MLCIN accumulation that can occur. Although MLCIN nearly doubles between 0000 UTC and 0300 UTC for both cases, the median values of 34 and 56 J kg^{-1} , respectively, are in good agreement with the median value of 50 J kg^{-1} for the Plains subset of nocturnal tornado cases in DF09. Moreover, the interquartile range for the sigtor cases is much smaller than that for the nontor events (i.e. $47\text{-}63 \text{ J kg}^{-1}$ versus $95\text{-}175 \text{ J kg}^{-1}$) at 0300 UTC, suggesting that the sigtor events generally occur within a narrow range of low MLCIN environments. Kis and Straka (2010) noted a distinct tendency for weaker buoyancy and increased near-ground static stability in significant nocturnal tornado events compared to similar afternoon events. However, our specific subset of Plains events reveals relatively weak MLCIN and large MLCAPE with significant tornadoes compared to nontornadic nocturnal episodes.

All other variables being equal, RB98, C02, T03 and more recently DF09 have shown that the probability of significant tornadoes increases with decreasing LCL heights. While not explicitly quantifying a physical process that directly relates to tornado formation, lower LCL heights are consistent with the hypothesis of Markowski et al. (2002) that increased low-level relative humidity (RH) may be associated with positive buoyancy in the rear flank downdraft outflow, and an increased probability of tornadoes. In our case sample, MLLCL heights are slightly lower for the sigtor cases for both times, though the differences are too small to be resolved in an operational forecast setting (Fig. 18). MLLCL heights lower by more than a quartile in both subsets between 0000 and 0300 UTC, which would

be expected given the observed boundary layer moistening (Fig. 16) and onset of radiational cooling. The median MLLCL value for the sigtor cases (993 m AGL at 0300 UTC) is in good agreement with both T03 (1004 m AGL for their sigtor events) and DF09 (996 m AGL for their Plains nighttime sigtor events).

The MLLFC (Fig. 19) discriminates more clearly between the sigtor and nontor cases than the MLLCL (Fig. 18). Similar to MLCIN (Fig. 17), this discrimination becomes even more apparent from 0000 UTC to 0300 UTC with the 90th percentile (relatively high values) of the sigtor cases falling below the 25th percentile (relatively low values) of the nontor cases. This observation can be expected, since MLCIN is indirectly accounted for by the MLLFC, whereby with increasing MLCIN, parcels have to be forced upward through a deeper layer of negative buoyancy before reaching their LFCs.

4.2 Kinematic Parameters

In addition to the three basic ingredients for thunderstorms, vertical wind shear represents an important fourth ingredient that is instrumental in determining the degree of storm organization. Cloud model simulations by Weisman and Klemp (1982), along with observational studies (e.g., Markowski et al. 1998; RB98; Bunkers 2002), indicate that a vector shear magnitude of roughly 15–20 m s⁻¹ over the lowest 6 km is necessary to support persistent, rotating updrafts. In Fig. 20, note that the interquartile range of the 0-6 km AGL vector shear magnitude for the sigtor cases is bound by a narrow range of 20-25 m s⁻¹; all of the sigtor cases are associated with supercells, and these environmental conditions are quite consistent with the results of Weisman and Klemp (1982), Markowski et al. 1998, RB98, and Bunkers 2002. Although the nontor cases have similar median values, the broader interquartile range might be symptomatic of a broader spectrum of convective storm types represented by this subset.

In addition to the prerequisite minimum 0-6 km vector shear magnitude of 15-20 m s⁻¹, Davies-Jones et al. 1990, Rasmussen (2003), T03, and DF09 all have shown that significantly tornadic supercells are typically associated with larger SRH than nontornadic supercells. Historically, SRH has been measured using fixed layers such as 0-1 or 0-3 km AGL. Recently, T07 developed a parameter that incorporates the thermodynamic characteristics (i.e. CAPE and CIN criteria of 100 J kg⁻¹ and -250 J kg⁻¹, respectively) of the lower troposphere in order to define an “effective inflow layer”. The SRH

calculated through the depth of the effective inflow layer was defined as the effective SRH (ESRH). T07 found ESRH to be an improved measure of low-level shear in elevated supercell environments, as well as a better discriminator between sigtor and nontor environments than fixed layer SRH calculations.

The results of this study are similar to that of T07. Whereas the 0-1 km SRH exhibited considerable overlap between the sigtor and nontor cases at both 0000 and 0300 UTC (Fig. 21), the ESRH (Fig. 22) shows considerably better discriminatory skill. This is particularly the case at 0300 UTC, where the 75th percentile of the nontor cases fall below the 25th percentile of the sigtor subset. This tendency is similar to that of MLCIN and MLLFC, which both account for negative parcel buoyancy in the low-level thermodynamic profile. Therefore, it appears that a better discrimination between the two subsets can be arrived at through the incorporation of low-level thermodynamic characteristics with an assessment of low-level shear.

Through the use of NPN and WSR-88D VAD data, an independent set of vector shear magnitude calculations was derived through the 0-1 and 0-6-km AGL layers. Although the temporal character of these observations is the same as that of the RUC proximity sounding data (0000 and 0300 UTC), the locations were close but not exact. Nonetheless, comparisons were made in order to assure that the computations were relatively close. The results shown in Figs. 23 and 24 indicate that the 0-6-km shear vector magnitude values were quite similar for the observed and RUC data at 0300 UTC. However, the 0-1-km shear vector magnitude for the observed NPN and WSR-88D VAD data were a quartile stronger than the RUC soundings. This likely is due to an underestimation of the LLJ magnitude by the RUC, a condition that has been recently observed in different configurations of the Weather Research and Forecasting (WRF) model as noted by Storm et al. (2009).

5. SUMMARY AND DISCUSSION

Based on the results of this study, it has been shown that the details of the synoptic pattern are quite similar for both the sigtor and nontor cases. The primary features associated with this pattern are a midlevel trough over the western United States, a developing or deepening lee cyclone in the lower troposphere over the central or southern High Plains and the development of a LLJ in the 0100-0300 UTC

timeframe. This LLJ development is earlier than that observed with the NBLWM under quiescent synoptic-scale conditions where an inertial oscillation in the lower troposphere is the primary forcing mechanism. It is hypothesized that the hastened acceleration of the LLJ is associated with synoptic or subsynoptic-scale forcing attendant to the documented large-scale pattern.

The LLJ has been identified as a critical component of this pattern as it serves to enhance potential instability locally through the poleward flux of heat and moisture. On average, MLCAPE was documented to *increase* between 0000 and 0300 UTC, which is contrary to the climatological diurnal tendency. Additionally, the development of the LLJ directly enhances vertical wind shear, particularly in the near-ground layer. Whereas the LLJ characteristics of the sigtor and nontor cases are similar, the thermodynamic characteristics, primarily in low levels, appear to be strong discriminators between the two environments. Through the use of RUC analysis soundings, it was determined that parameters that account for negative parcel buoyancy in the low-levels such as MLCIN, MLLFC, and ESRH most strongly discriminate between the two environments. Moreover, the discriminatory value of these parameter fields improve from 0000 to 0300 UTC, suggesting that the presence of a more moist boundary layer in the sigtor cases likely slows radiational cooling and the associated development of the nocturnal inversion.

Another interesting aspect of these documented sigtor cases is that they typically precede the progression of the primary mid-level trough east of the Rockies within 24 h. As a result, ensuing major severe weather outbreaks have followed a number of these events by less than twenty-four hours and, in some cases, over the same geographic region as the nocturnal tornadoes. A good example of this is the 4 and 5 May 2007 sequence where regional severe weather outbreaks occurred over the Great Plains, with the most intense storms focused over western and central parts of Kansas (not shown). Although the 5 May event was more widespread (including more tornadoes), the 4 May Greensburg, KS tornado was the highest impact event of the two-day sequence.

Often the anticipation of the next day's severe weather potential can overshadow the comparatively more isolated, but possibly more significant threat to life and property leading up to these events. Moreover, these nocturnal tornado episodes represent a noticeable departure from the

late afternoon climatological peak in Plains tornadoes, when relatively unobstructed visibility aids in storm spotting and public severe weather warnings. As a result, it is hoped the results of this study will allow for more reliable and accurate forecasts of these events which present a great challenge to the integrated warning system (Doswell et al. 1999).

ACKNOWLEDGEMENTS

The authors would like to thank Chuck Doswell for several enlightening discussions, a thorough review of the initial manuscript, and his encouragement throughout this project. Roger Edwards (SPC) contributed to initial project design, and Steve Weiss (SPC) provided numerous suggestions for improvement via a detailed review of the manuscript.

6. REFERENCES

- Ashley, W. S., 2007: Spatial and temporal analysis of tornado fatalities in the United States: 1880-2005. *Wea Forecasting*, **22**, 1214-1228.
- Beebe, R. G., 1955: Types of air masses in which tornadoes occur. *Bull. Amer. Meteor. Soc.*, **36**, 349-350.
- Beebe, R. G., 1958: Tornado proximity soundings. *Bull. Amer. Meteor. Soc.*, **39**, 195-201.
- Beebe, R. G., and F. C. Bates, 1955: A mechanism for assisting in the release of convective instability. *Mon. Wea. Rev.*, **83**, 1-10.
- Benjamin, S. G., and Coauthors, 2002: RUC20 –The 20-km version of the Rapid Update Cycle. NOAA Tech. Memo. OAR FSL twentyeight. Forecast Systems Laboratory, Boulder, CO, 9 pp.
- Benjamin, S. G., and Coauthors, 2004: An hourly assimilation-forecast cycle: The RUC. *Mon. Wea. Rev.*, **132**, 495-518.
- Blackadar, A. K., 1957: Boundary layer wind maxima and their significance for the growth of nocturnal inversions, *Bull. Amer. Meteor. Soc.*, **38**, 283-290.
- Bluestein, H. B., E. W. McCaul Jr., G. P. Byrd, and G. R. Woodall, 1988: Mobile sounding observations of a tornadic storm near the

- dryline: The Canadian, Texas storm of 7 May 1986. *Mon. Wea. Rev.*, **116**, 1790–1804.
- Bluestein, H. B., E. W. McCaul Jr., G. P. Byrd, G. R. Woodall, G. Martin, S. Keighton, and L. C. Showell, 1989: Mobile sounding observations of a thunderstorm near the dryline: The Gruver, Texas storm complex of 25 May 1987. *Mon. Wea. Rev.*, **117**, 244–250.
- Bonner, W. D., 1965: Statistical and kinematic properties of the low-level jet stream. Res. Pap. 38, Satellite and Mesometeorology Project, University of Chicago, 54 pp.
- Bonner, W. D., 1966: Case study of thunderstorm activity in relation to the low-level jet. *Mon. Wea. Rev.*, **94**, 167-178.
- Bonner, W. D., 1968: Climatology of the low-level jet. *Mon. Wea. Rev.*, **96**, 833-850.
- Brooks, H. E., C. A. Doswell III, and J. Cooper, 1994a: On the environments of tornadic and nontornadic mesocyclones. *Wea. Forecasting*, **9**, 606–618.
- Brooks, H. E., C. A. Doswell III, and M. P. Kay, 2003: Climatological estimates of local daily tornado probability for the United States. *Wea. Forecasting*, **18**, 626-640.
- Bunkers, M. J., 2002: Vertical wind shear associated with left-moving supercells. *Wea. Forecasting*, **17**, 845–855.
- Carlson, T. N., S. G. Benjamin, G. S. Forbes, Y. F. Li, 1983: Elevated mixed layers in the regional severe storm environment: Conceptual model and case studies. *Mon. Wea. Rev.*, **111**, 1453-1474.
- Colby, F. P., 1984: Convective inhibition as a predictor of convection during AVE-SESAME-2. *Mon. Wea. Rev.*, **112**, 2239-2252.
- Concannon, P. R., H. E. Brooks, and C. A. Doswell III, 2000: Climatological risk of strong and violent tornadoes in the United States. Preprints, *Second Conf. on Environmental Applications*, Long Beach, CA, Amer. Meteor. Soc., 212-219.
- Craven, J. P., H. E. Brooks, and J. A. Hart, 2002a: Baseline climatology of sounding derived parameters associated with deep, moist convection. Preprints, *21st Conf. on Severe Local Storms*, San Antonio, TX, Amer. Meteor. Soc., 643–646.
- Craven, J. P., R. E. Jewell, and H. E. Brooks, 2002b: Comparison between observed convective cloud-base heights and lifting condensation level for two different lifted parcels. *Wea. Forecasting*, **17**, 885–890.
- Darkow, G. L., and D. W. McCann, 1977: Relative environmental winds for 121 tornado bearing storms. Preprints, *10th Conf. on Severe Local Storms*, Omaha, NE, Amer. Meteor. Soc., 413–417.
- Davies, J. M., 2004: Estimations of CIN and LFC associated with tornadic and nontornadic supercells. *Wea. Forecasting*, **19**, 714-726.
- Davies, J. M. and R. H. Johns, 1993: Some wind and instability parameters associated with strong and violent tornadoes. 1. Wind shear and helicity. *The Tornado: Its Structure, Dynamics, Prediction, and Hazards, Geophys. Monogr.*, No. 79, Amer. Geophys. Union, 573–582.
- Davies, J. M. and A. Fischer, 2009: Environmental characteristics associated with nighttime tornadoes. *NWA Electronic Journal of Operational Meteorology*, 2009-EJ3.
- Davies-Jones, R. P., 1984: Streamwise vorticity: The origin of updraft rotation in supercell storms, *J. Atmos. Sci.*, **41**, 2991-3006.
- Davies-Jones, R. P., D. W. Burgess, and M. Foster, 1990: Test of helicity as a tornado forecast parameter, Preprints, 16th Conf. on Severe Local Storms, pp. 588-592, American Meteorological Society, Boston, Mass.
- desJardins M. L., K. F. Brill, and S. S. Schotz, 1991: GEMPAK 5. Part 1-GEMPAK 5 programmer's guide. National Aeronautics and Space Administration, 176 pp. [Available from Scientific and Technical Information Division, Goddard Space Flight Center, Greenbelt, MD 20771.].
- Doswell, C. A., III, and E. N. Rasmussen, 1994: The

- effect of neglecting the virtual temperature correction on CAPE calculations. *Wea. Forecasting*, **9**, 625–629.
- Doswell, C. A., III, H. E. Brooks, and R. A. Maddox, 1996: Flash flood forecasting: An ingredients-based methodology. *Wea. Forecasting*, **11**, 360–381.
- Doswell, C. A., III, A. R. Moller, and H. E. Brooks, 1999: Storm spotting and public awareness since the first tornado forecasts of 1948. *Wea. Forecasting*, **14**, 544–557.
- Doswell, C. A., III, and D. M. Schultz, 2006: On the use of indices and parameters in forecasting severe storms. *Electronic J. Severe Storms Meteor.*, **1**(3), 1–22.
- Fischer, A. and J. M. Davies, 2009: Significant Nighttime Tornadoes in the Plains Associated with Relatively Stable Low-Level Conditions. *NWA Electronic Journal of Operational Meteorology*, 2009-EJ4.
- Hane, C. E., M. E. Baldwin, H. B. Bluestein, T. M. Crawford, R. M. Rabin, 2001: A case study of severe storm development along a dryline within a synoptically active environment. part I: dryline motion and an eta model forecast. *Mon. Wea. Rev.*, **129**, 2183–2204.
- Hart, J. A., and J. Korotky, 1991: The SHARP Workstation V1.50. A skew-t/hodograph analysis and research program for the IBM and compatible PC. Users manual, NOAA. [Available from NOAA, National Weather Service, Eastern Region HQS, 630 Johnson Ave., Bohemia, NY 11716-2626].
- Hoecker, W. H., 1961: Three southerly low level jet systems delineated by the Weather Bureau special pibal network. *Mon. Wea. Rev.*, **91**, 573–582.
- Holton, J. R., 1967: The diurnal boundary-layer wind oscillation above sloping terrain. *Tellus*, **19**, 199–205.
- Johns, R. H., J. M. Davies, and P. W. Leftwich, 1993: Some wind and instability parameters associated with strong and violent tornadoes. 2. Variations in the combinations of wind and instability parameters. *The Tornado: Its Structure, Dynamics, Prediction, and Hazards, Geophys. Monogr.*, No. 79, Amer. Geophys. Union, 583–590.
- Kis, A. K. and J. M. Straka, 2010: Nocturnal tornado climatology. *Wea. Forecasting*, **25**, 545–561.
- Kelly, D. L., J. T. Schaefer, R. P. McNulty, C. A. Doswell III, and R. F. Abbey, Jr., 1978: An augmented tornado climatology. *Mon. Weather Rev.*, **106**, 1172–1183.
- Lemon, L.R. and M. Umschied, 2008: The Greensburg, Kansas Tornadic Storm: A Storm of Extremes. Preprints, 24th Conf. Severe Local Storms, Savannah, GA. Amer. Meteor. Soc. 2.4
- Lilly, D. K., 1983: Dynamics of rotating thunderstorms, in *Mesoscale Meteorology—Theories, Observations and Models*, edited by D. K. Lilly and T. gal.-Chen, pp. 531–543, D. Reidel, Hingham, Mass., 1983.
- Lilly, D. K., 1986: The structure, energetics and propagation of rotating convective storms, II, Helicity and storm stabilization, *J. Atmos. Sci.*, **43**, 126–140.
- Maddox, R. A., 1976: An evaluation of tornado proximity wind and stability data. *Mon. Wea. Rev.*, **104**, 133–142.
- Maddox, R. A., 1993: The diurnal low-level wind oscillation and storm-relative helicity. *Proc., Tornado Symp. III*, C. Church, Ed., Amer. Geo-phys. Union.
- Markowski, P. N., J. M. Straka, E. N. Rasmussen, and D. O. Blanchard, 1998: Variability of storm-relative helicity during VORTEX. *Mon. Wea. Rev.*, **126**, 2959–2971.
- Markowski, P. N., J. M. Straka, and E. N. Rasmussen, 2002: Direct surface thermodynamic observations within the rear-flank downdrafts of nontornadic and tornadic supercells. *Mon. Wea. Rev.*, **130**, 1692–1721.
- Means, L. L., 1952: On thunderstorm forecasting in the central United States. *Mon. Wea. Rev.*, **80**, 165–189.
- Means, L. L., 1954: A study of the mean southerly

- wind maxima in low levels associated with a period of summer precipitation in the middle west. *Bull. Amer. Meteor. Soc.*, **35**, 166-170.
- Miller, R. C., 1972: Notes on analysis and severe storm forecasting procedures of the Air Force Global Weather Central. Air Weather Service Tech. Rep. 200 (Rev.), 190 pp. [Available from Air Weather Service, AWS/XTX, Scott Air Force Base, IL 62225-5438.]
- Moncrief, M., and M. J. Miller, 1976: The dynamics and simulation of tropical cumulonimbus and squall lines. *Quart. J. Roy. Meteor. Soc.*, **102**, 373-394.
- Potvin, C. K., K. L. Elmore, and S. J. Weiss, 2010: Assessing the impact of proximity sounding criteria on the climatology of significant tornado environments. Accepted to *Wea. Forecasting*.
- Rasmussen, E. N., and D. O. Blanchard, 1998: A baseline climatology of sounding-derived supercell and tornado forecast parameters. *Wea. Forecasting*, **13**, 1148-1164.
- Reiter, E. R., 1969: Tropopause circulation and jet streams. *World Survey of Climatology*, Vol. 4, *Climate of the Free Atmosphere*, D. F. Rex, Ed., Elsevier, 85-193.
- Roebber, P.J., D.M. Schultz and R. Romero, 2002: Synoptic Regulation of the 3 May 1999 Tornado Outbreak. *Wea. Forecasting*, **17**, 399-429.
- Rotunno, R. and J. B. Klemp, 1982: The influence of the shear-induced pressure gradient on thunderstorm motion. *Mon. Wea. Rev.*, **110**, 136-151.
- Showalter, A. K., and J. R. Fulks, 1943: Preliminary report on tornadoes. U.S. Weather Bureau, 162 pp.
- Storm, B., J. Dudhia, S. Basu, A. Swift, and I. Giammanco, 2009: Evaluation of the Weather Research and Forecasting model on forecasting low-level jets: implications for wind energy, *Wind Energy* **12**, 81-90, DOI: 10.1002/we.288.
- Thompson, R. L., J. M. Lewis, and R. A. Maddox, 1994: Autumnal return of tropical air to the Gulf of Mexico's coastal plain. *Wea. Forecasting*, **9**, 348-360.
- Thompson, R. L., R. Edwards, J. A. Hart, K. L. Elmore, and P. Markowski, 2003: Close proximity soundings within supercell environments obtained from the Rapid Update Cycle. *Wea. Forecasting*, **18**, 1243-1261.
- Thompson, R. L., C. M. Mead, and R. Edwards, 2007: Effective storm-relative helicity and bulk shear in supercell thunderstorm environments. *Wea. Forecasting*, **22**, 102-115.
- Uccellini, L. W. 1980: On the role of upper tropospheric jet streaks and leeside cyclogenesis in the development of low-level jets in the Great Plains. *Mon. Wea. Rev.*, **108**, 1689-1696.
- Uccellini, L. W., 1990: The relationship between jet streaks and severe convective storm systems. Preprints, *16th Conf. on Severe Local Storms*, Kananaskis Park, AB, Canada, Amer. Meteor. Soc., 121-130.
- Uccellini, L. W., and D. R. Johnson, 1979: The coupling of upper and lower tropospheric jet streaks and implications for the development of severe convective storms. *Mon. Wea. Rev.*, **107**, 682-703.
- Wexler, H., 1961: A boundary layer interpretation of the low-level jet. *Tellus*, **13**, 368-378.

7. TABLES AND FIGURES

Event Date	Location	Number of nocturnal EF2+ tornadoes	Strongest nocturnal tornado	Touchdown time of the strongest nocturnal tornado (UTC)
3 May 1999	north-central OK	11	EF4	2:25
3 June 1999	south-central NE	2	EF3	4:19
4 June 1999	north-central NE	2	EF2	2:22
17 May 2002	northwest OK	2	EF3	4:32
21 April 2001	southwest KS	1	EF4	2:15
7 May 2003	south-central OK	3	EF2	7:54
9 May 2003	central OK	1	EF3	3:28
23 June 2003	northeast NE	1	EF4	2:43
12 May 2004	south-central KS	3	EF4	1:39
11 May 2005	southwest KS	1	EF2	2:02
2 April 2006	southwest KS	1	EF2	2:19
20 April 2007	southwest NE	2	EF2	3:02
4 May 2007	southwest KS	4	EF5	2:00
23 May 2007	TX panhandle	2	EF2	3:50
24 April 2008	north-central KS	1	EF2	5:23
25 April 2009	north-central OK	2	EF2	3:10

Table 1. Listing of the 16 significant nocturnal tornado events identified for this study. Violent tornado occurrences are in bold.

Mean value	Sigtor (00 UTC)	Sigtor (03 UTC)	Nontor (00 UTC)	Nontor (03 UTC)
MLMIXR (g kg^{-1})	12.1	13.9	10.9	12.0
MLCAPE (J kg^{-1})	2159	2770	1635	1809
MLCIN (J kg^{-1})	-54	-55	-88	-158
MLLCL (m AGL)	1448	1006	1585	1145
MLLFC (m AGL)	2364	1975	2839	2750
3-6 km AGL LR (C km^{-1})	7.6	7.5	7.8	7.9
Effective SRH ($\text{m}^2 \text{s}^{-2}$)	188	395	146	231
0-1 km SRH ($\text{m}^2 \text{s}^{-2}$)	169	345	140	305
0-1 km vector shear mag. (m s^{-1})	10.0	15.5	8.5	14.0
Effective vector shear mag. (m s^{-1})	24.5	23.5	22.0	20.5
0-6 km vector shear mag. (m s^{-1})	23.5	23.0	22.0	21.0

Table 2. Mean values for a select number of thermodynamic and kinematic parameters for the sigtor and nontor sub sets at 00 and 03 UTC.

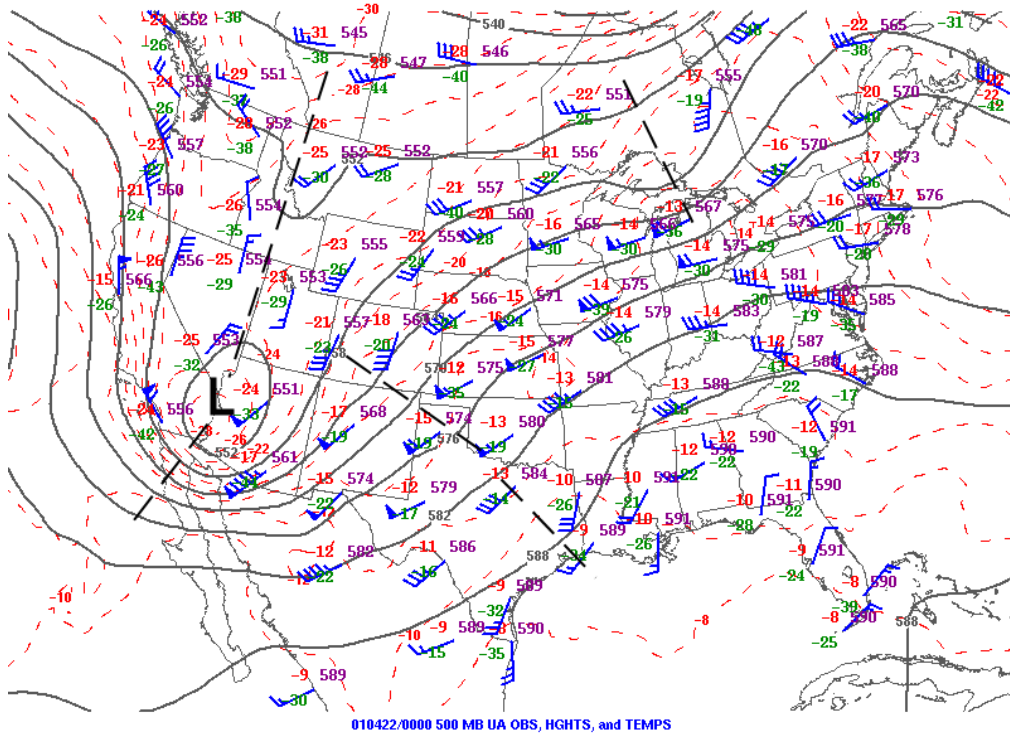


Figure 1a. Annotated 500 hPa upper-air analysis valid 0000 UTC 22 April 2001.

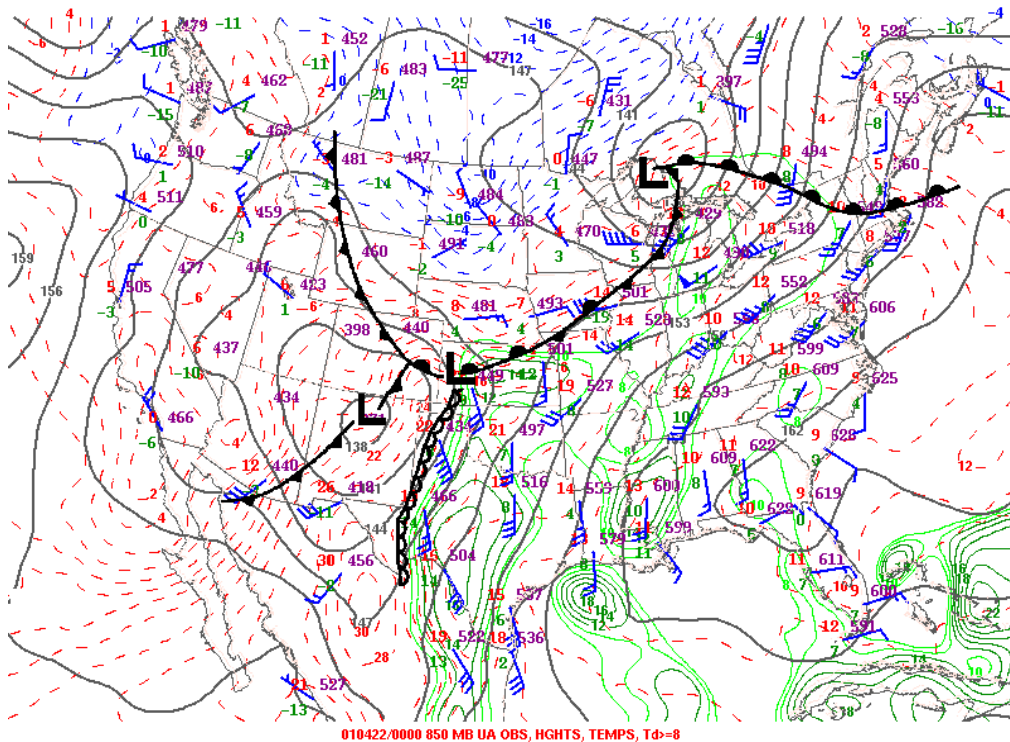


Figure 1b. Same as Fig. 1a, except for 850 hPa with conventional frontal symbols.

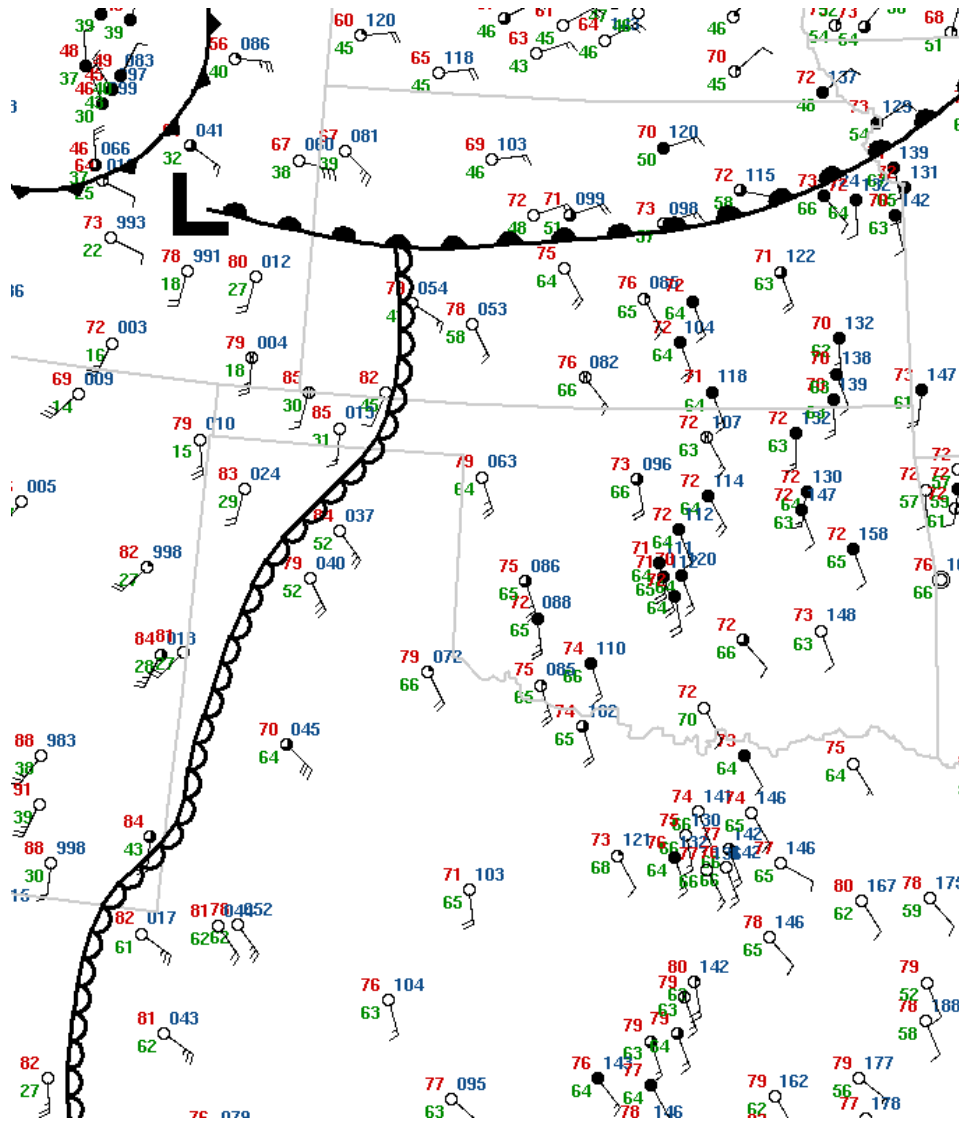


Figure 1c. Surface station model plot valid 0000 UTC 22 April 2001, annotated with conventional frontal symbols.

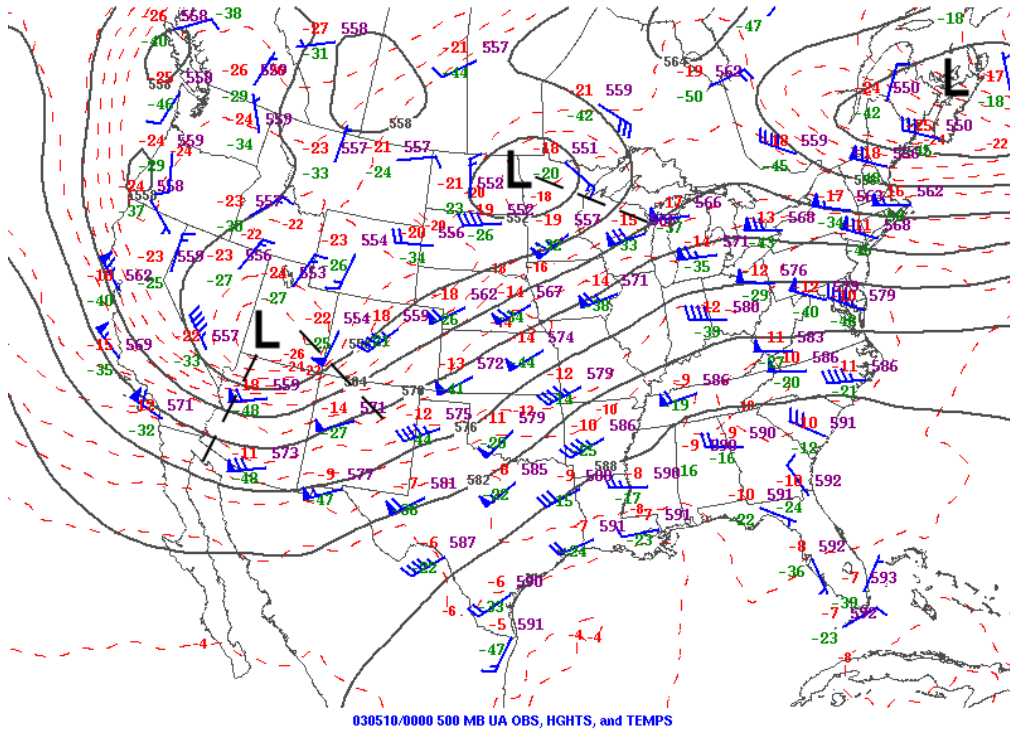


Figure 2a. Same as Fig. 1a, except for analysis valid at 0000 UTC 10 May 2003.

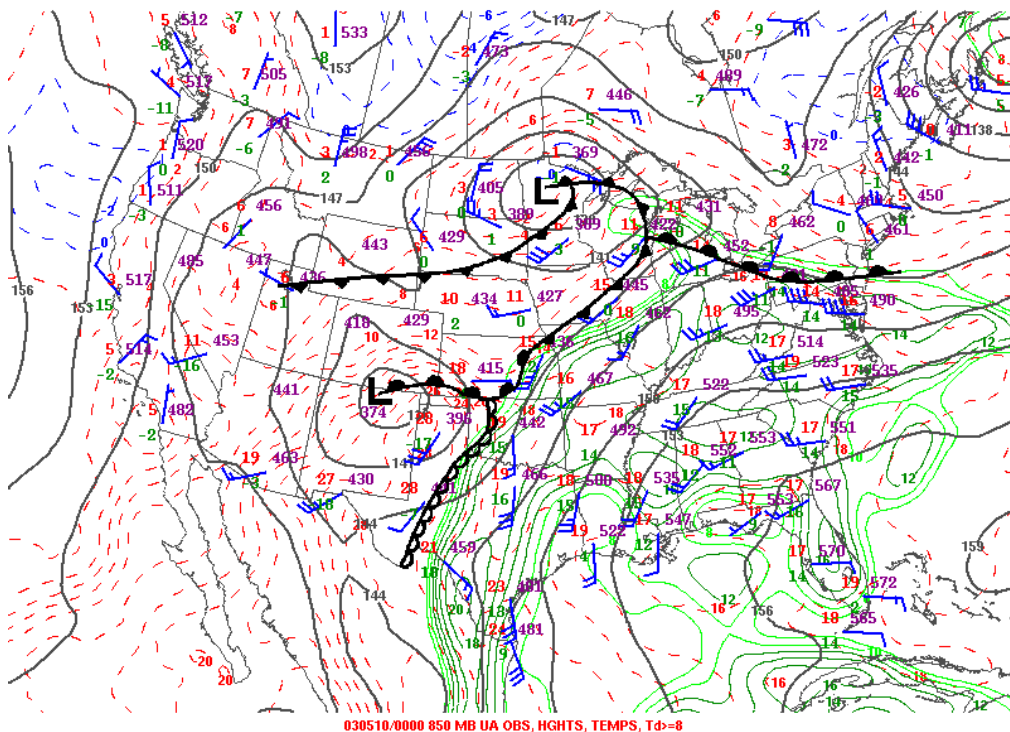


Figure 2b. Same as Fig. 1b., except for analysis valid at 0000 UTC 10 May 2003.

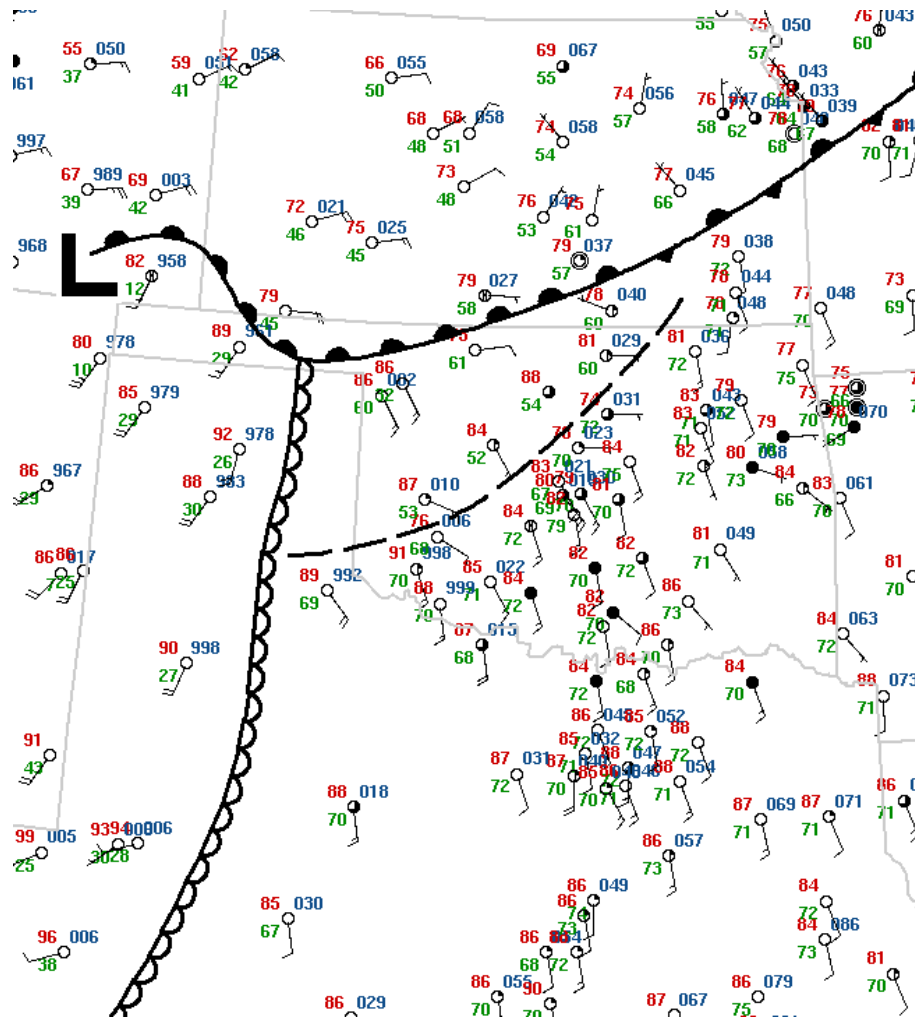


Figure 2c. Surface station model plot valid 0000 UTC 10 May 2003 (conventions the same as Fig. 1c). The dashed line delineates a northwestward moving moisture discontinuity.

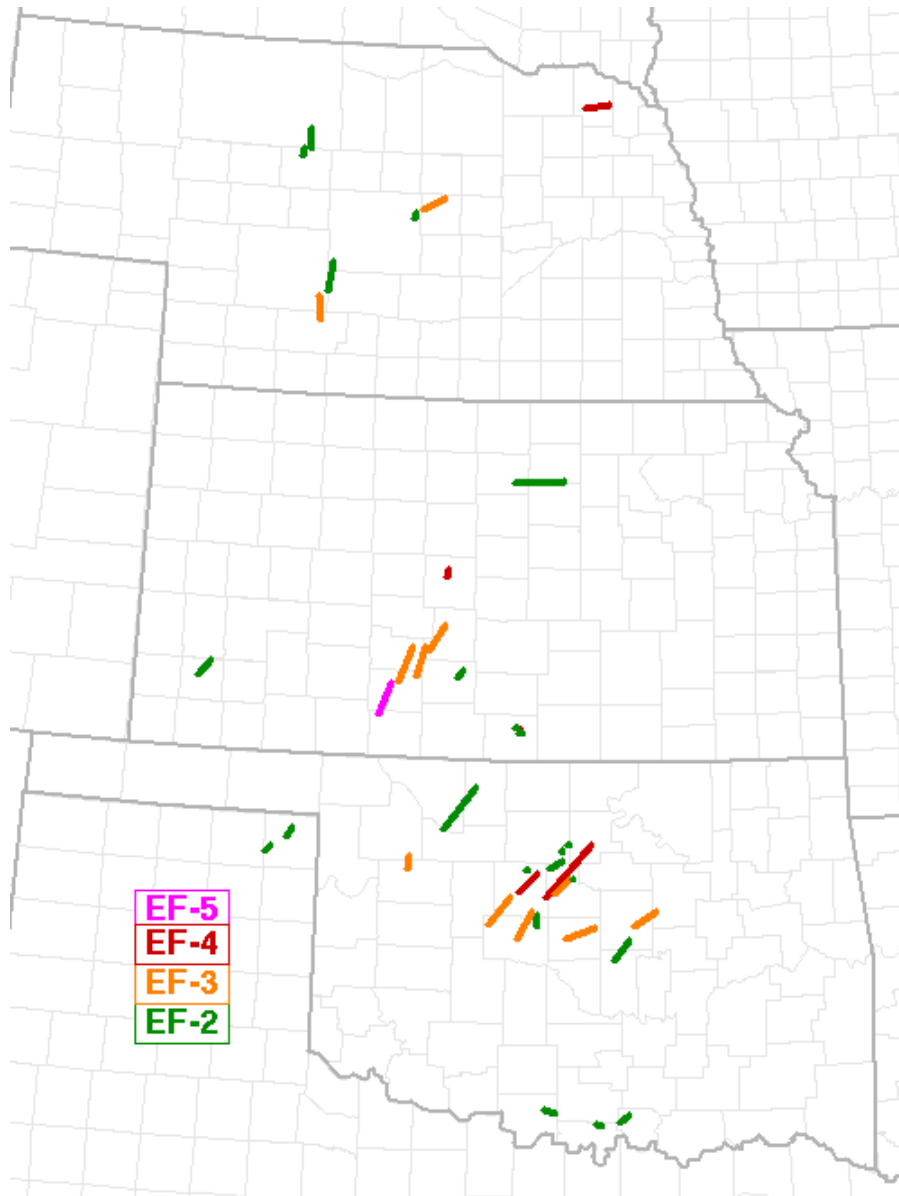


Figure 3. Graphical depiction of the nocturnal significant tornadoes included in this study. Tracks are color-coded by EF-scale.

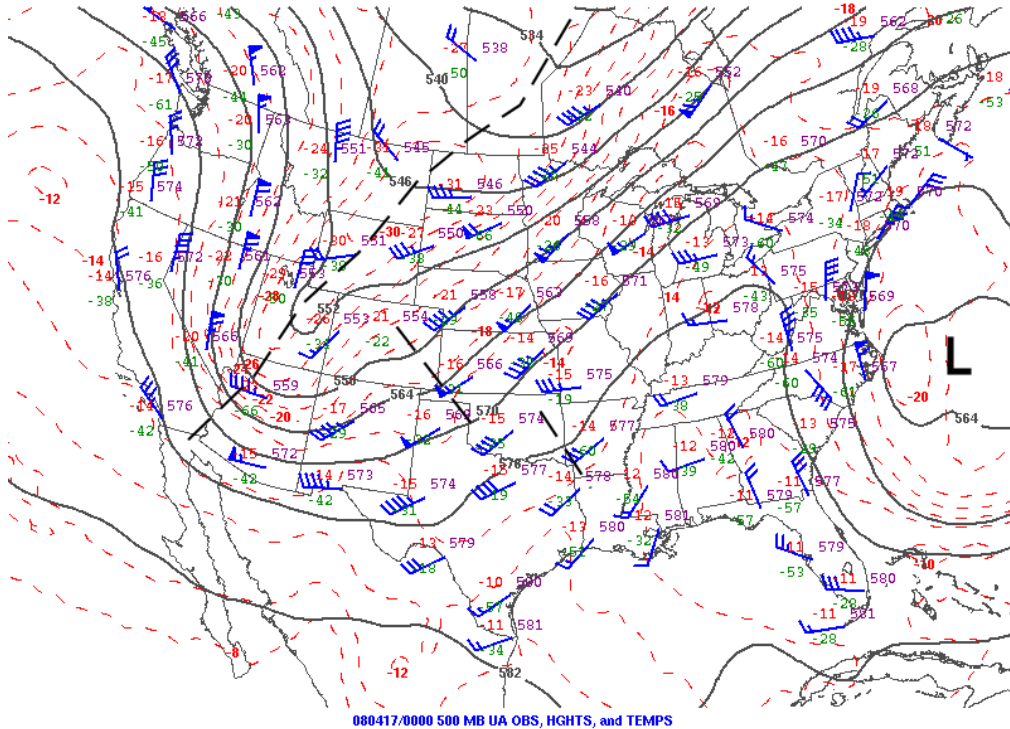


Figure 4a. Annotated 500 hpa upper-air analysis valid 0000 UTC 17 April 2008.

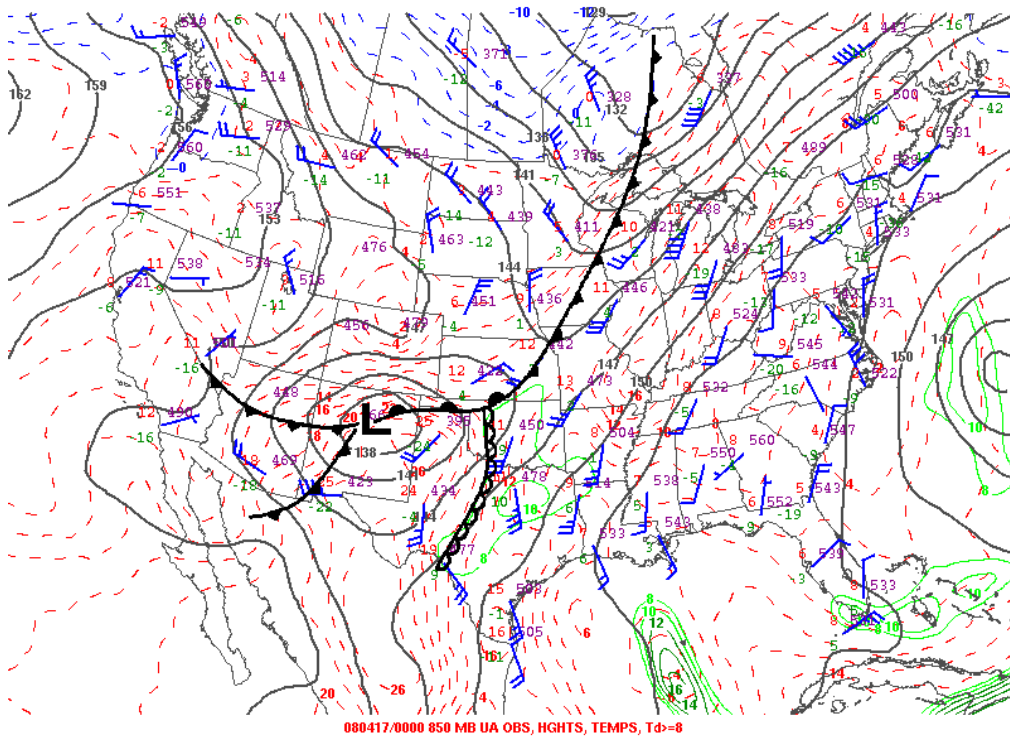


Figure 4b. Same as Fig. 4a, except for 850 hPa.

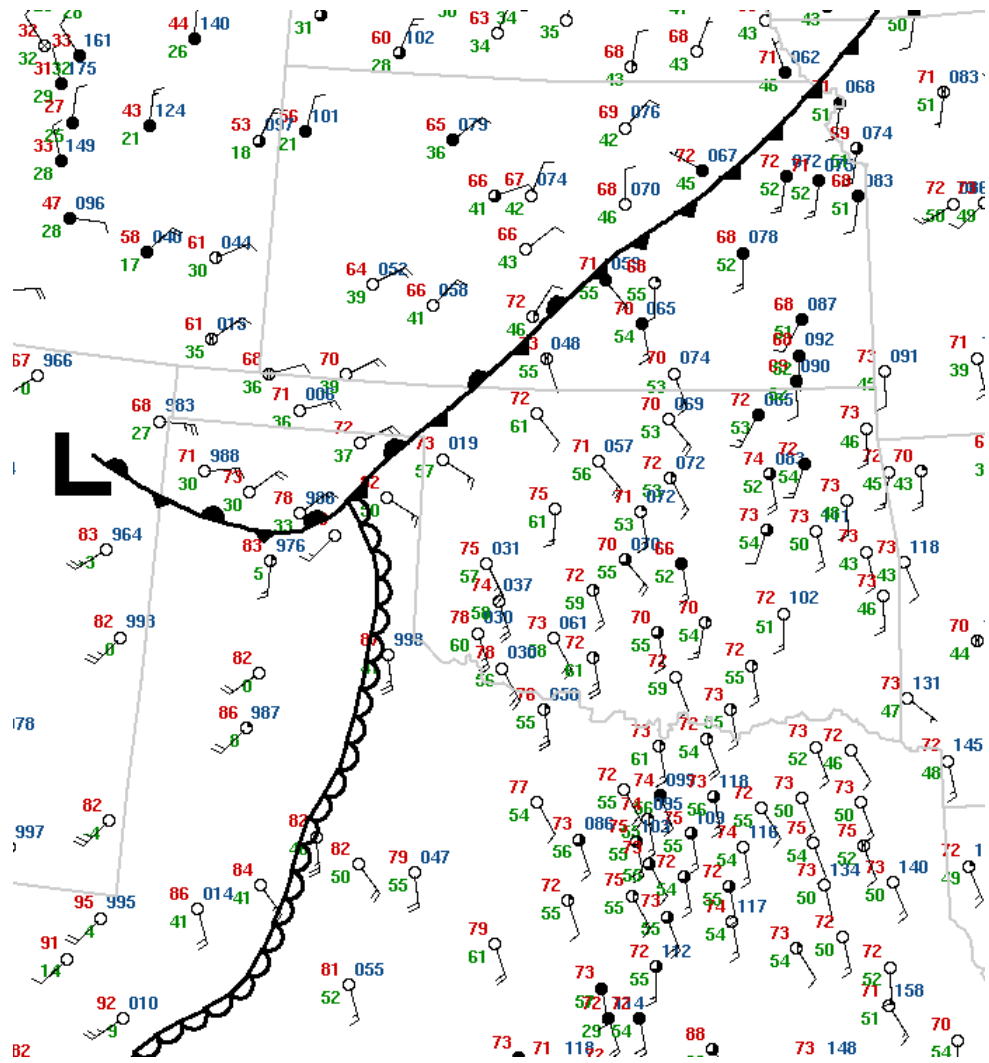


Figure 4c. Annotated surface map valid 0000 UTC 17 April 2008.

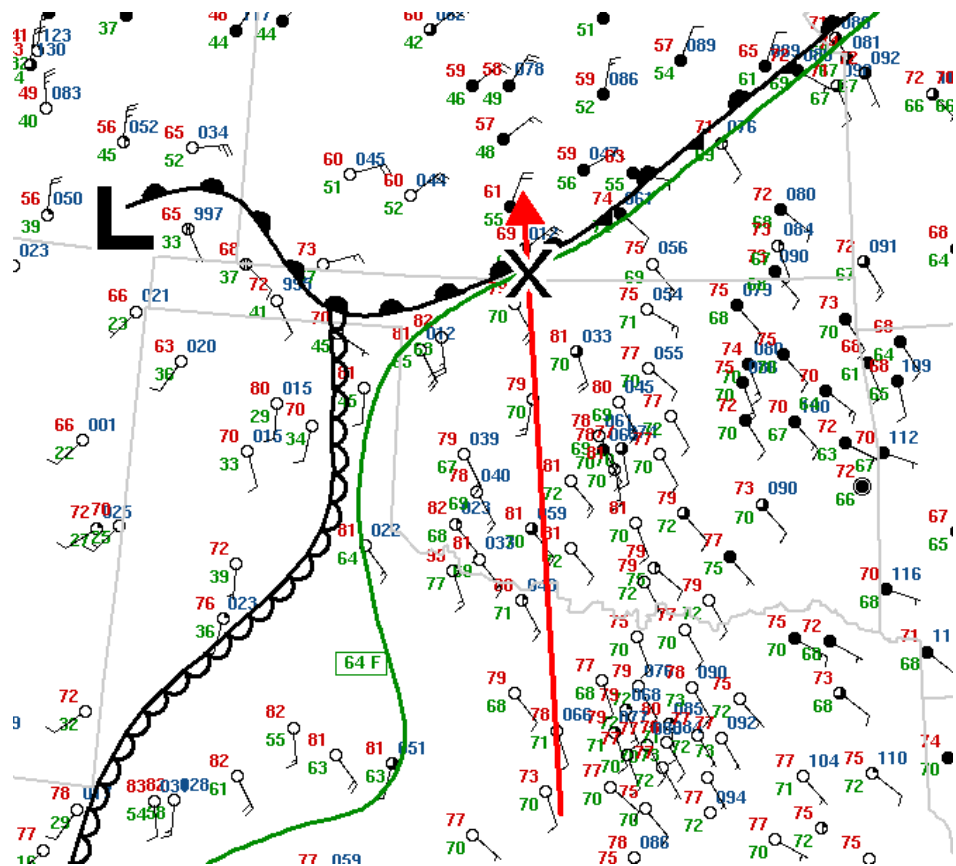
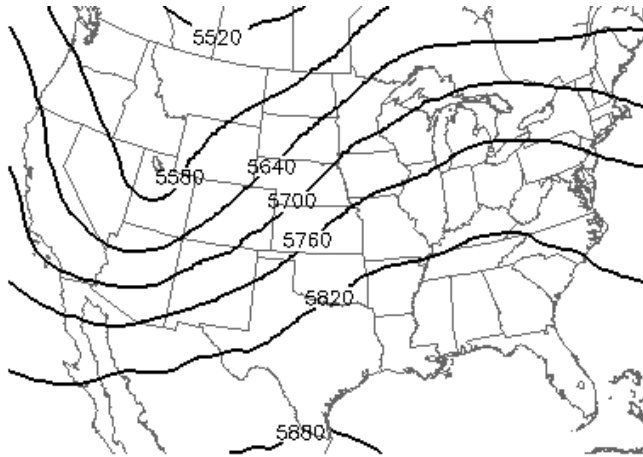
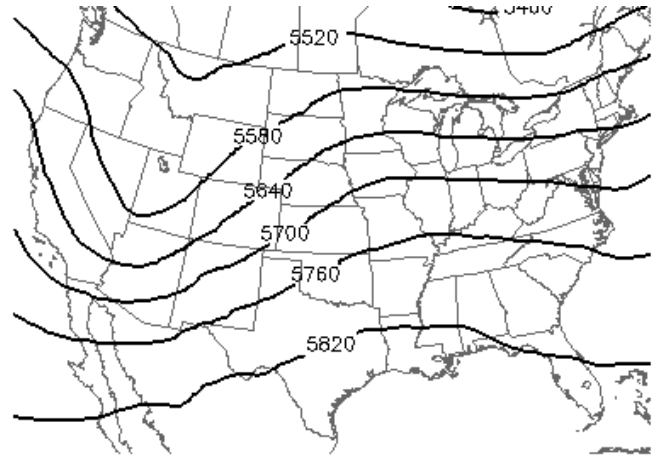


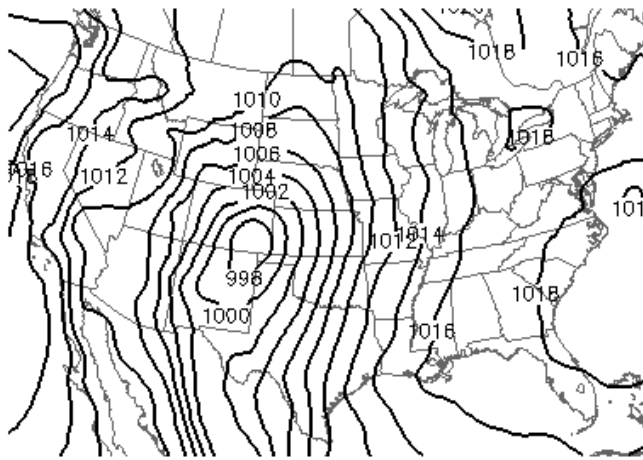
Figure 5. Sample case analysis consisting of the LLJ axis (red line with the arrowhead) superimposed on the surface map which includes standard frontal symbols and our subjectively-defined bound of the warm sector (green line), valid 0300 on UTC 13 May 2004. RUC analysis soundings were generated at the location of where the LLJ axis intersected the northern edge of the warm sector as denoted by the “X.”



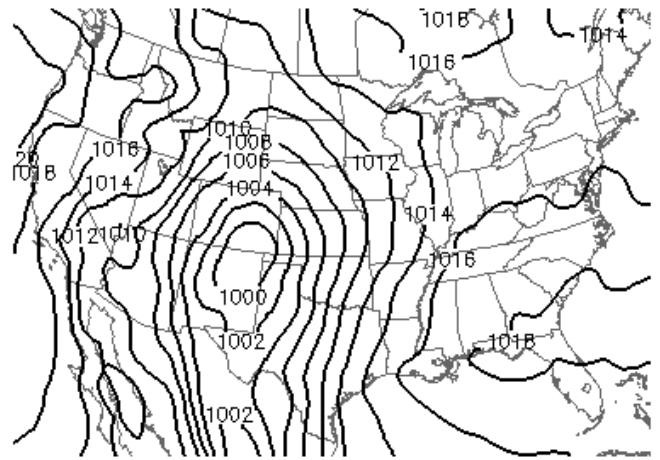
Mean 500 hPa height at 0000 UTC (in m – SIGTOR)



Mean 500 hPa height at 0000 UTC (in m – NONTOR)



Mean PMSL at 0000 UTC (in hPa – SIGTOR)



Mean PMSL at 0000 UTC (in hPa – NONTOR)

Figure 6. 0-hr RUC analysis grids, valid 0000 UTC, of mean 500 hPa geopotential heights (in meters - top) and mean sea-level pressure (in hPa - bottom) for the sigtor cases (left) and nontor cases (right).

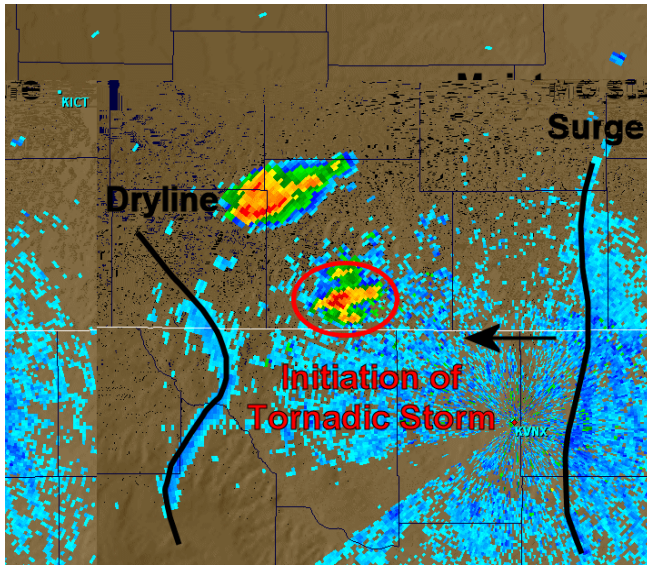


Figure 7a. KVNK WSR-88D reflectivity data at 0.5 degrees, valid 2321 UTC on 12 May 2004. The image depicts the formative stage of a tornadic storm which initiated along a bulging segment of the dryline. The storm later interacted with a westward-moving fineline which denoted a transition to a more moist, unstable boundary layer.

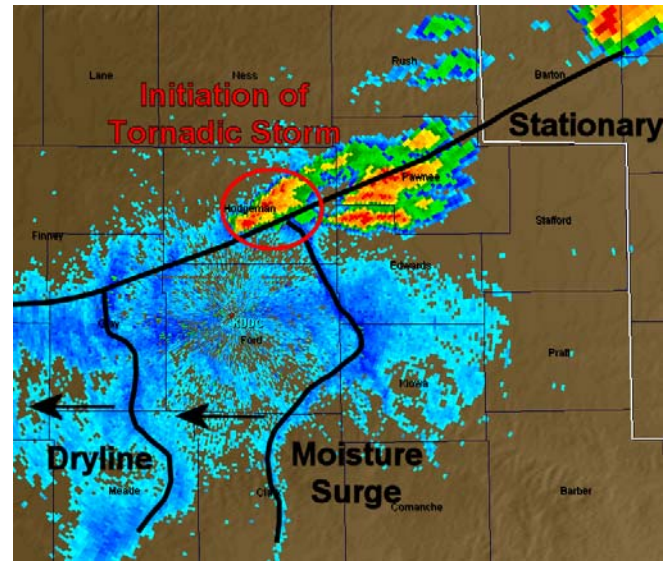


Figure 7b. KDDC WSR-88D reflectivity data at 0.5 degrees, valid 2344 UTC on 21 April 2001. The image depicts the formative stage of a tornadic storm which initiated near the intersection of a stationary or warm front with a westward-moving fineline which denoted a transition to a more moist, unstable boundary layer.

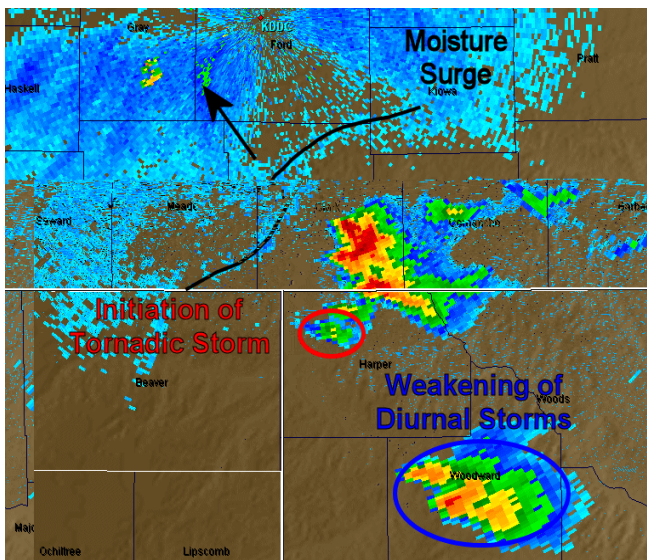


Figure 7c. KDDC WSR-88D reflectivity data at 0.5 degrees, valid 0042 UTC on 5 May 2007. The image depicts the formative stage of a tornadic storm which initiated along a northwestward-moving fineline which denoted a transition to a more moist, unstable boundary layer. Also shown is a weakening diurnal storm cluster which had earlier produced a tornado over far northwest Oklahoma.

Annual Distribution

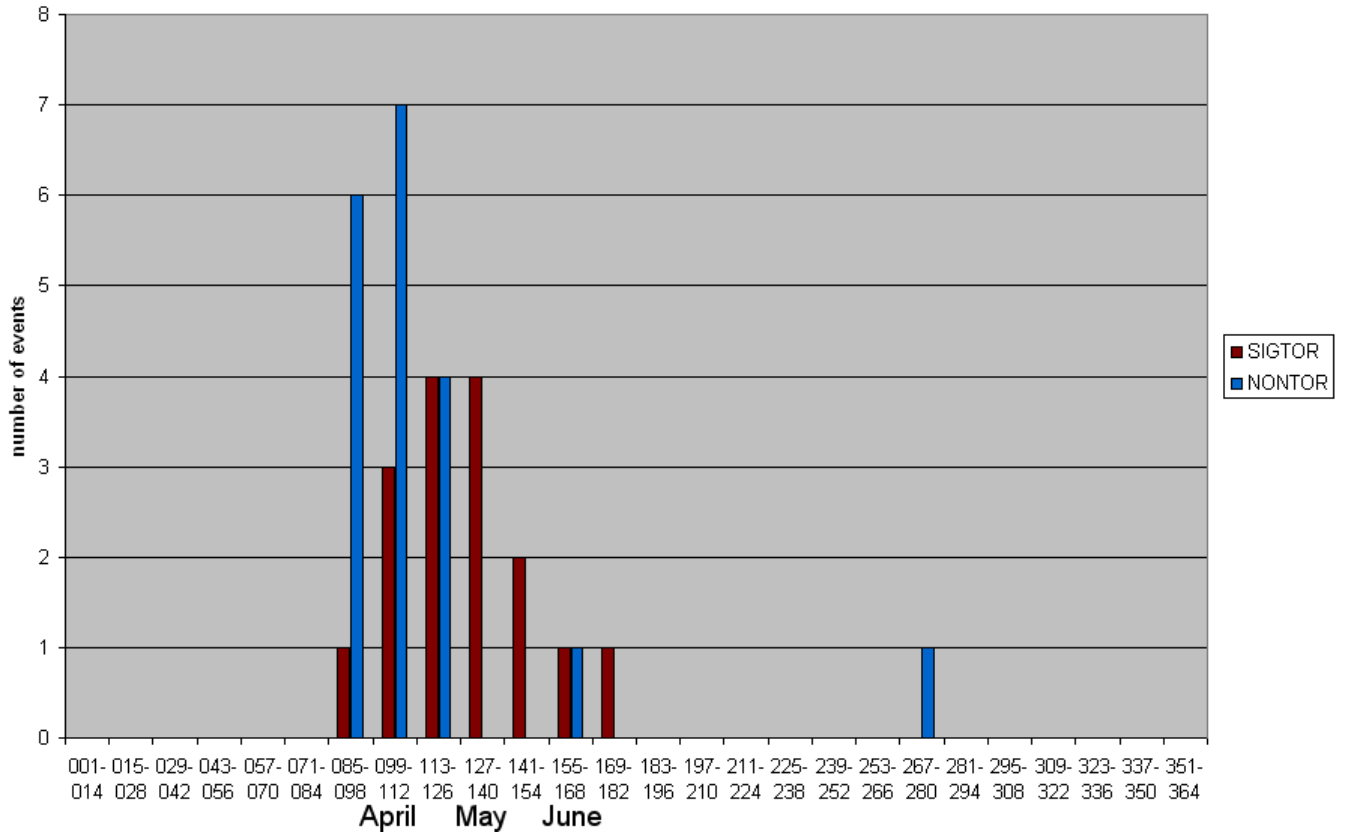
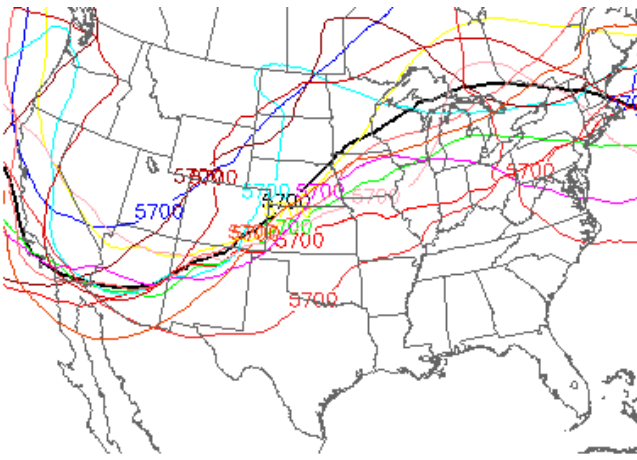
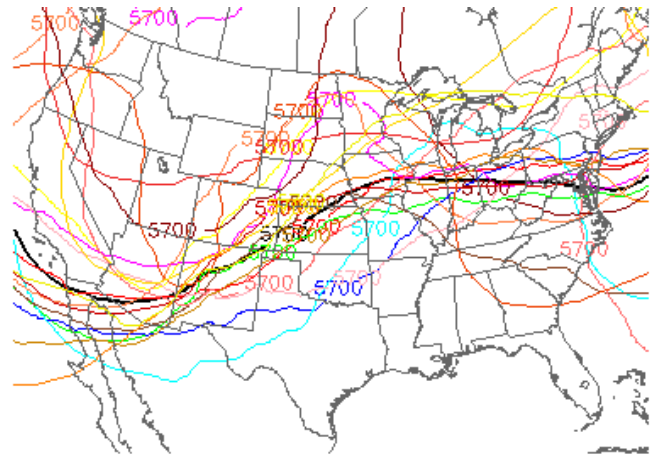


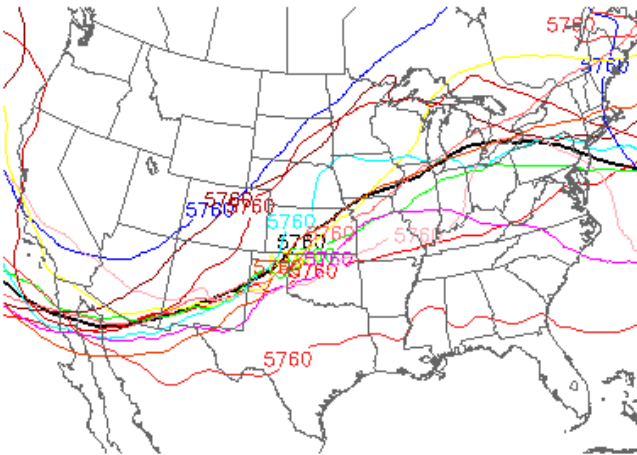
Figure 8. The annual distribution of the 35 cases in this study, binned bi-weekly by Julian day.



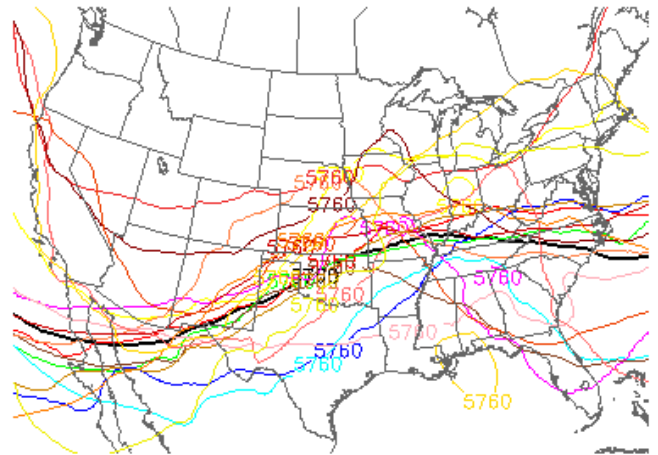
5700 m isoheight valid 0000 UTC (SIGTOR)



5700 m isoheight valid 0000 UTC (NONTOR)



5760 m isoheight valid 0000 UTC (SIGTOR)



5760 m isoheight valid 0000 UTC (NONTOR)

Figure 9. Spaghetti plots of 0-hr RUC analysis geopotential isoheights, valid at 0000 UTC, at 5700 meters (top) and 5760 meters (bottom). Individual sigtor cases are shown on the left with the nontor cases on the right.

Change in LLJ Magnitude with Time

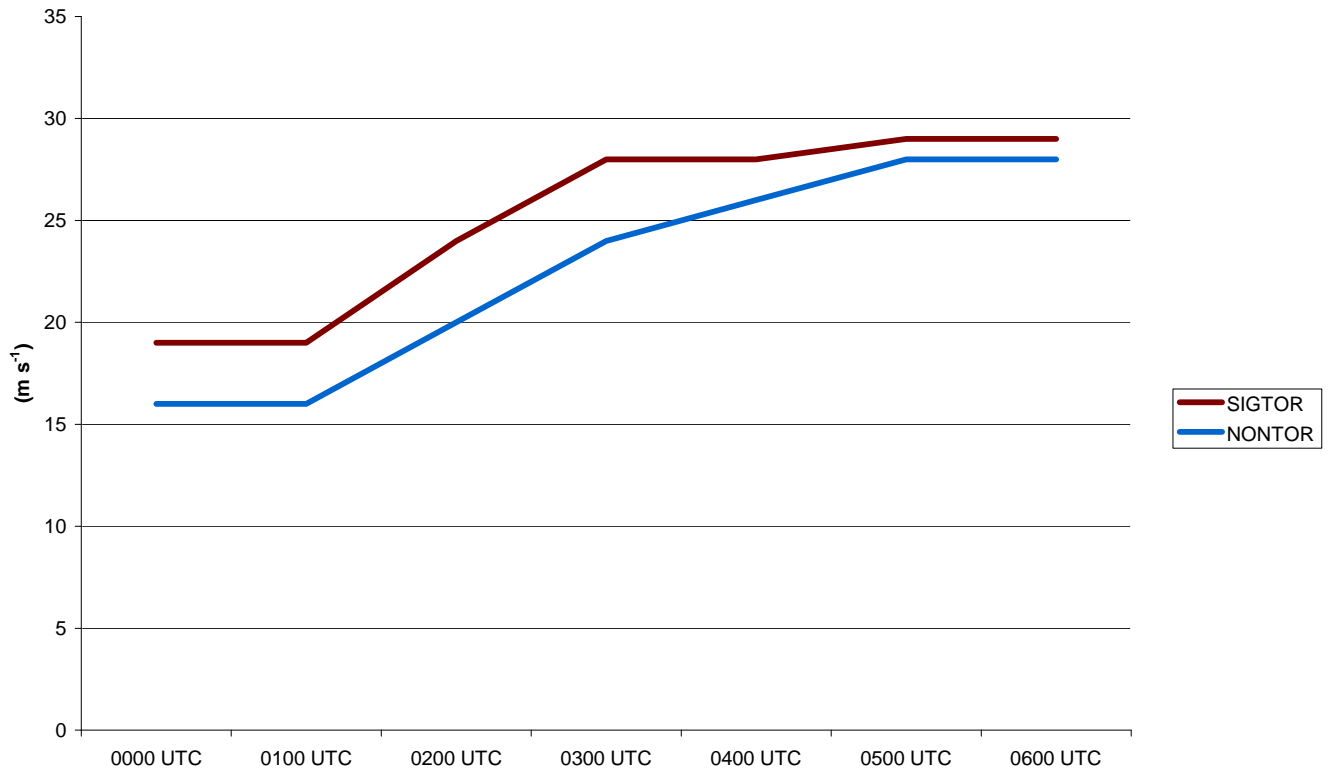
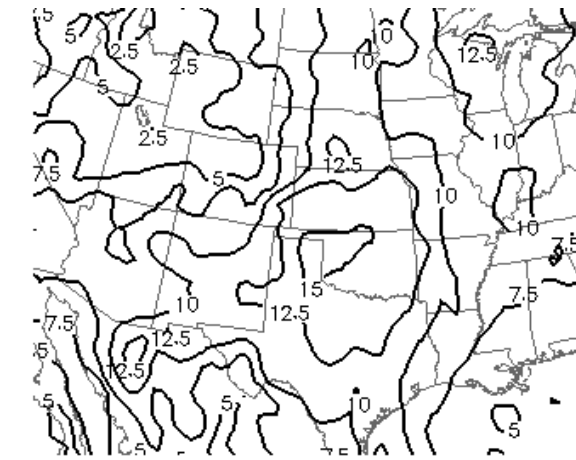
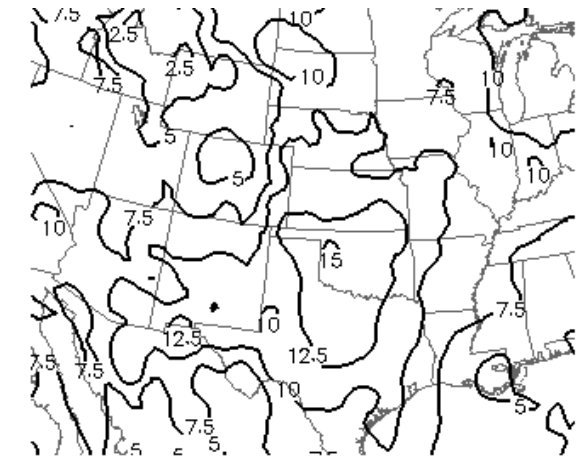


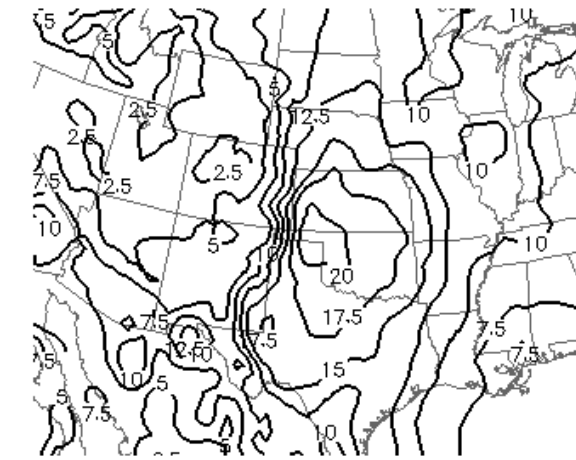
Figure 10. LLJ magnitude time-rate-of-change, based on NPN and WSR-88D VAD observations, for the sigtor and nontor cases.



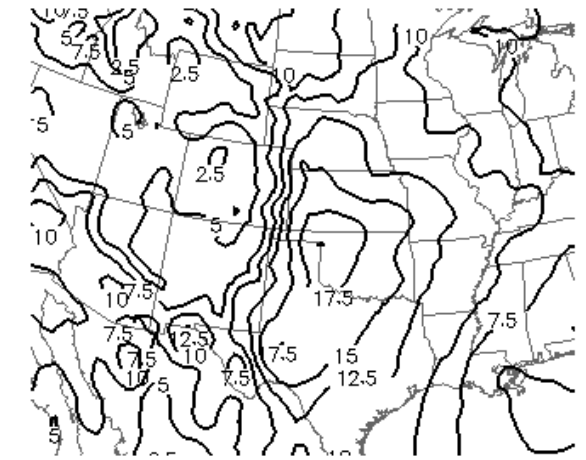
850 hPa isotachs at 0000 UTC ($m\ s^{-1}$ SIGTOR)



850 hPa isotachs at 0000 UTC ($m\ s^{-1}$ NONTOR)



850 hPa isotachs at 0300 UTC ($m\ s^{-1}$ SIGTOR)



850 hPa isotachs at 0300 UTC ($m\ s^{-1}$ NONTOR)

Figure 11. 0-hr RUC analysis grids of mean 850 mb isotachs ($m\ s^{-1}$), valid 0000 UTC (top) and 0300 UTC (bottom), for the sigtor cases (left) and the nontor cases (right).

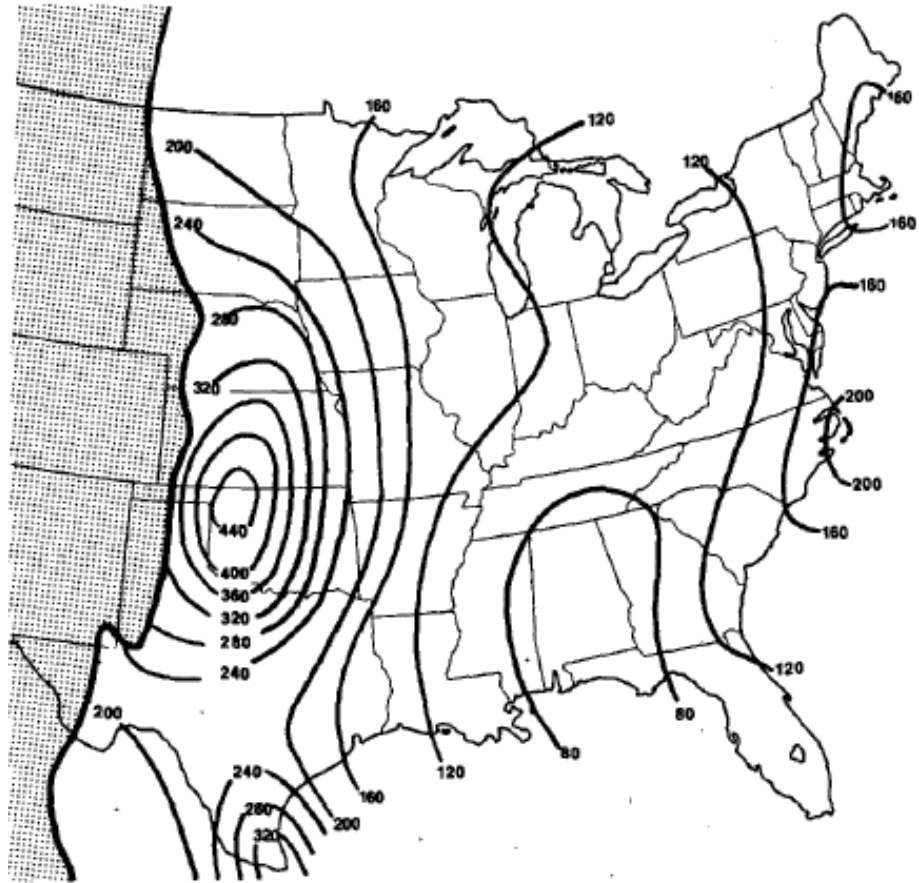


Figure 12. Number of low-level jet observations from January 1959-December 1960 at 1200 and 0000 UTC (from Bonner, 1965).

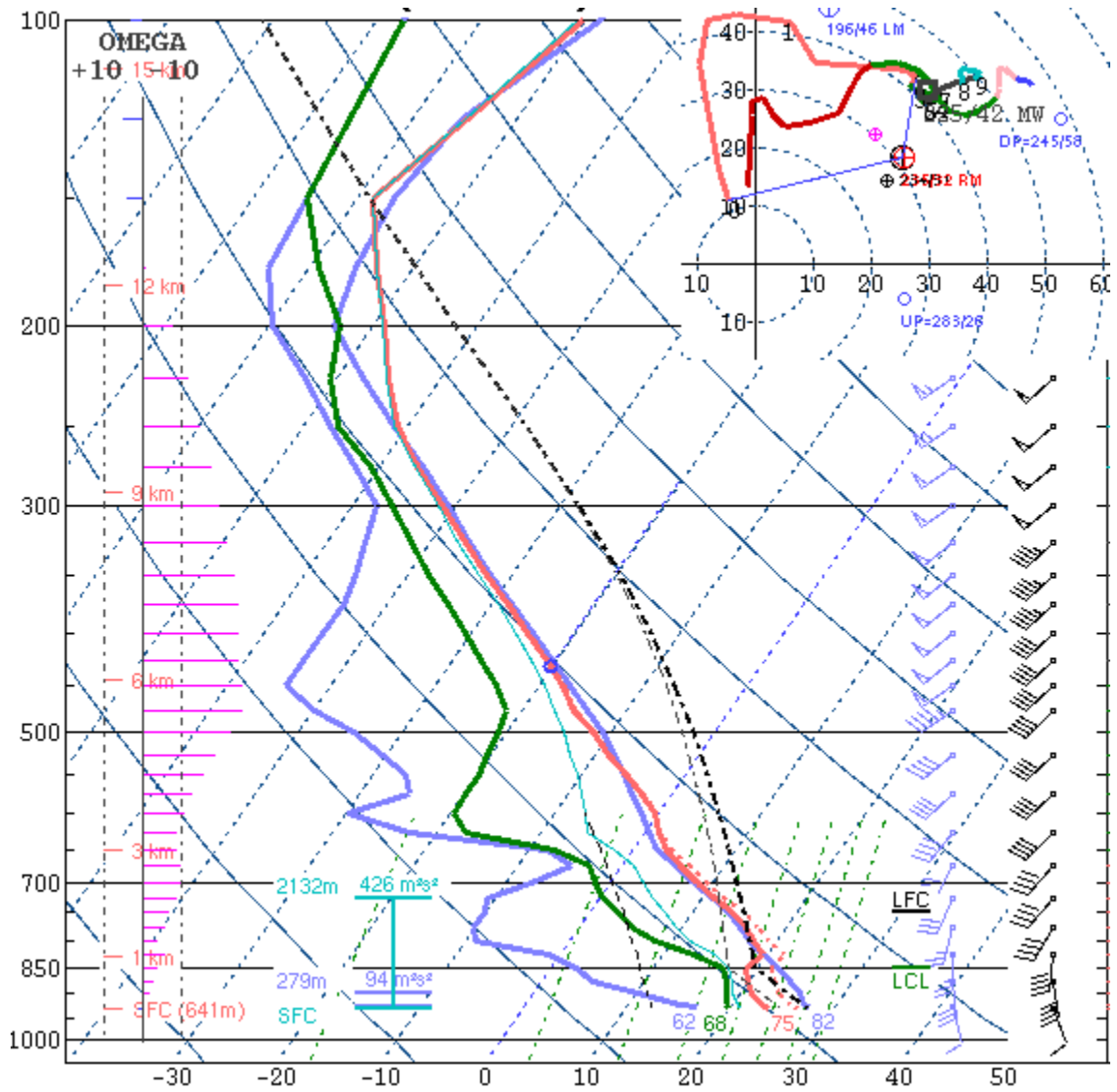


Figure 13. Overlay of 0-hr RUC analysis profiles for Pratt, KS, valid 0000 UTC (purple) and 0400 UTC on 5 May 2007. The lowest 3 km of the hodograph for the 0300 UTC profile is in light red.

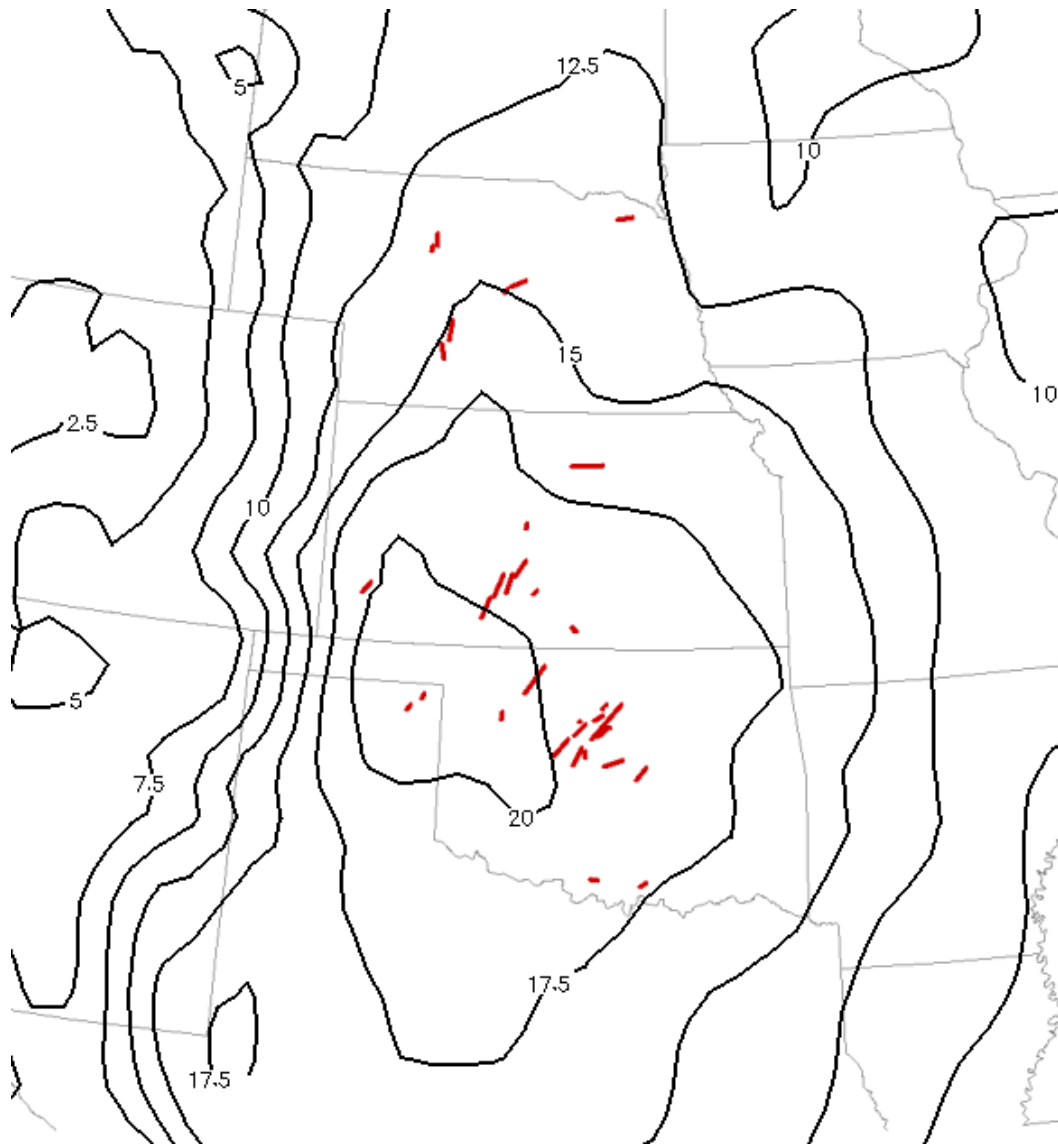


Figure 14. Composite of the sigtor tracks and the 0-hr RUC analysis grid of mean 850 hPa isotachs (m s^{-1}), valid 0300 UTC.

MLCAPE

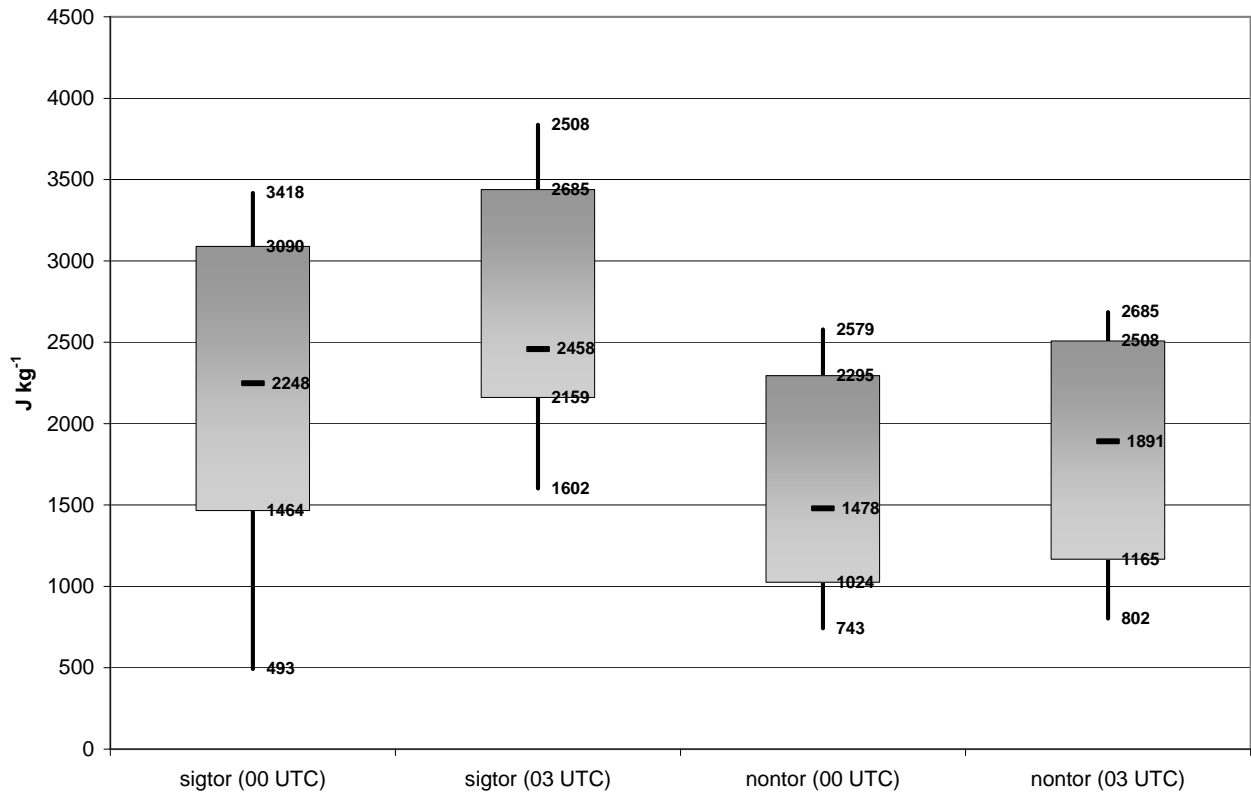


Figure 15. Box and whisker diagram of the 100-hPa (mb) mean parcel CAPE (MLCAPE, J kg⁻¹) for the sigtor (16) and nontor (19) cases. The shaded box covers the 25th–75th percentiles, the whiskers extend to the 10th and 90th percentiles, and the median values are marked by the heavy horizontal line within each shaded box.

ML Mixing Ratio

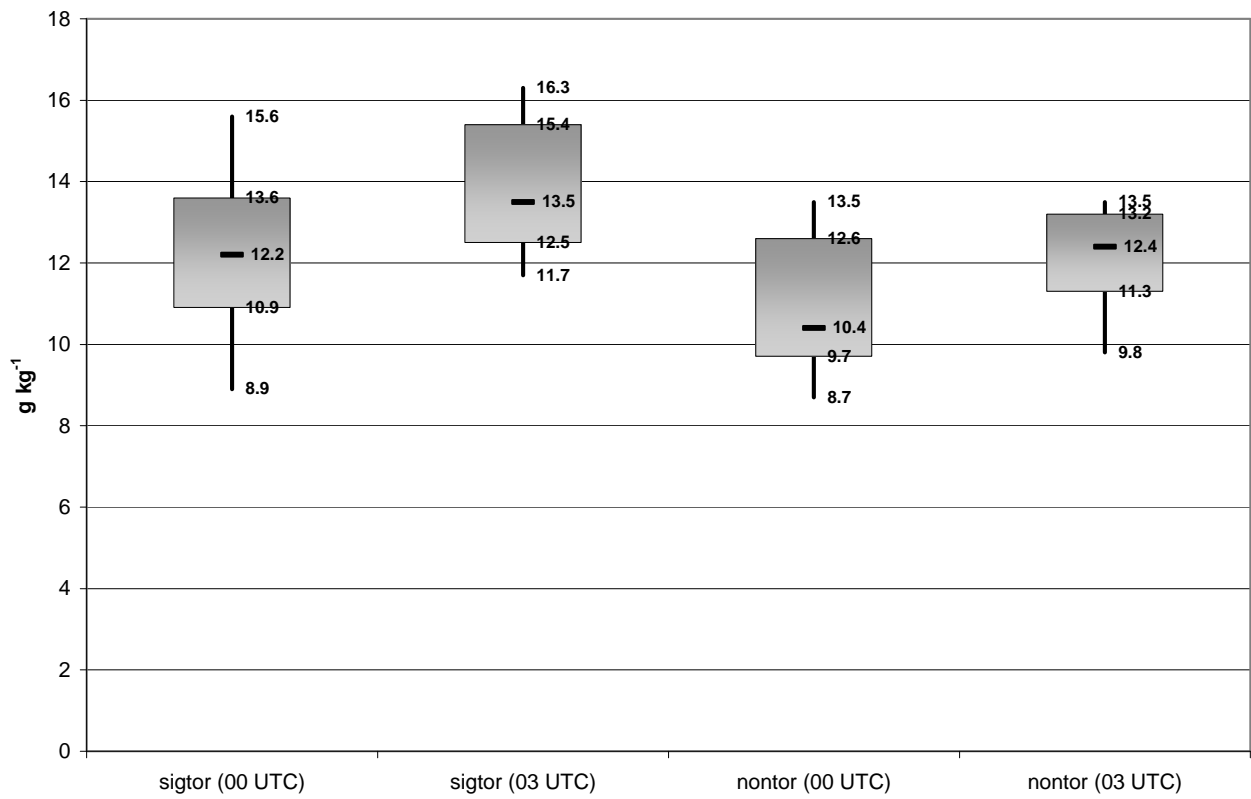


Figure 16. Same as Fig. 14, except for ML mixing ratio (g kg^{-1}).

MLCIN

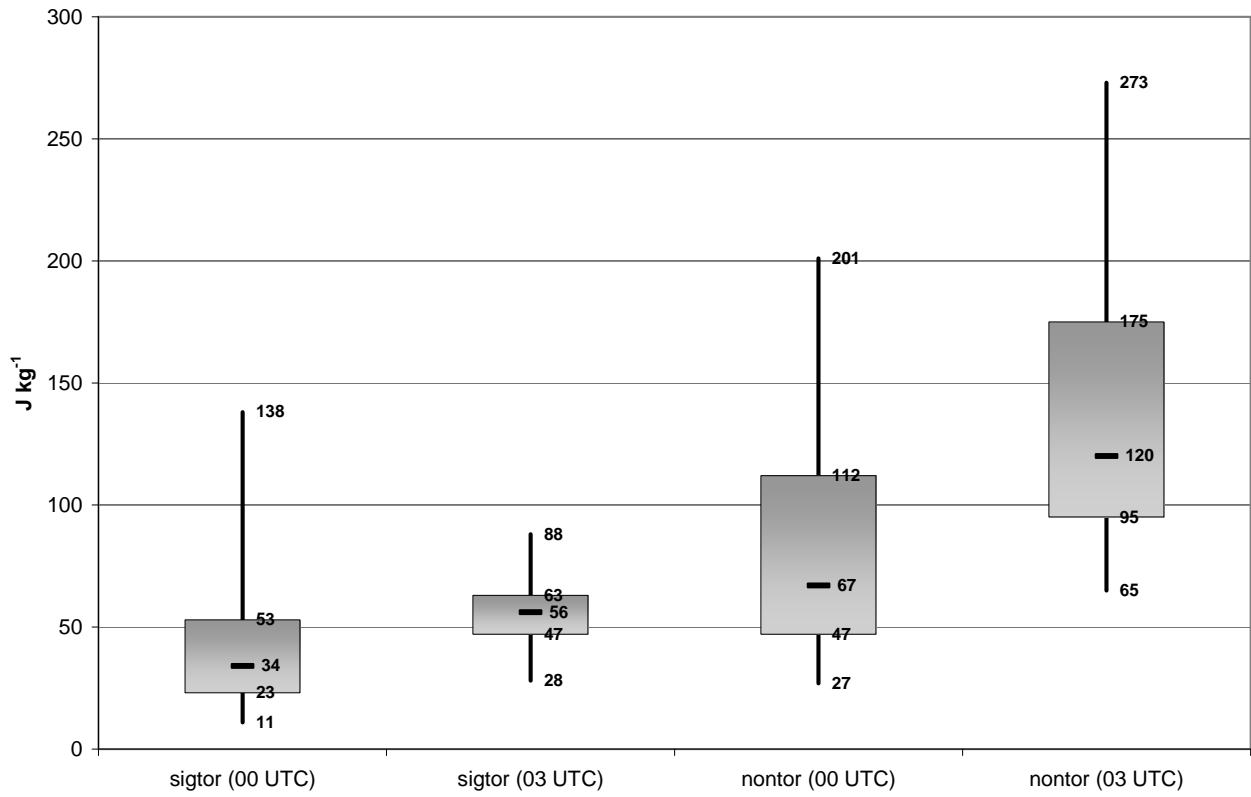


Figure 17. Same as Fig. 14, except for the absolute value of MLCIN (J kg^{-1}).

MLLCL

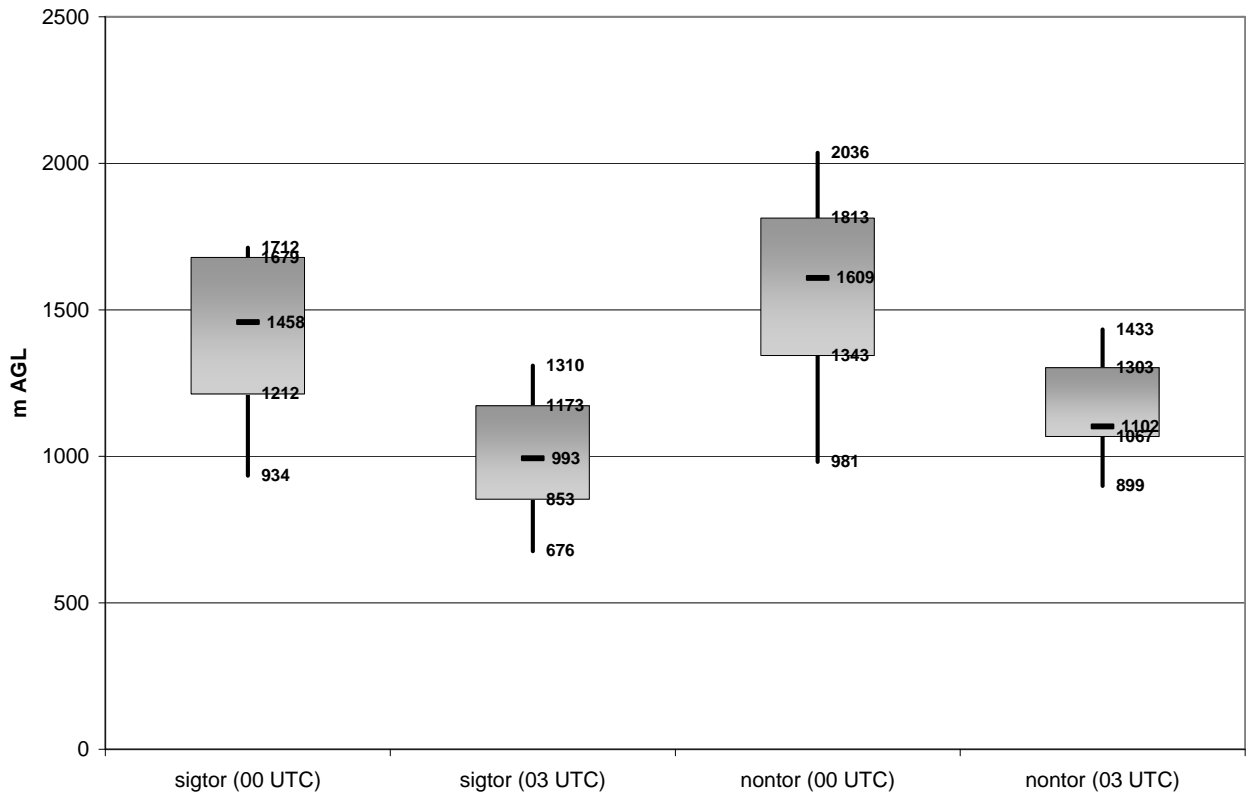


Figure 18. Same as Fig. 14, except for MLLCL (m AGL).

MLLFC

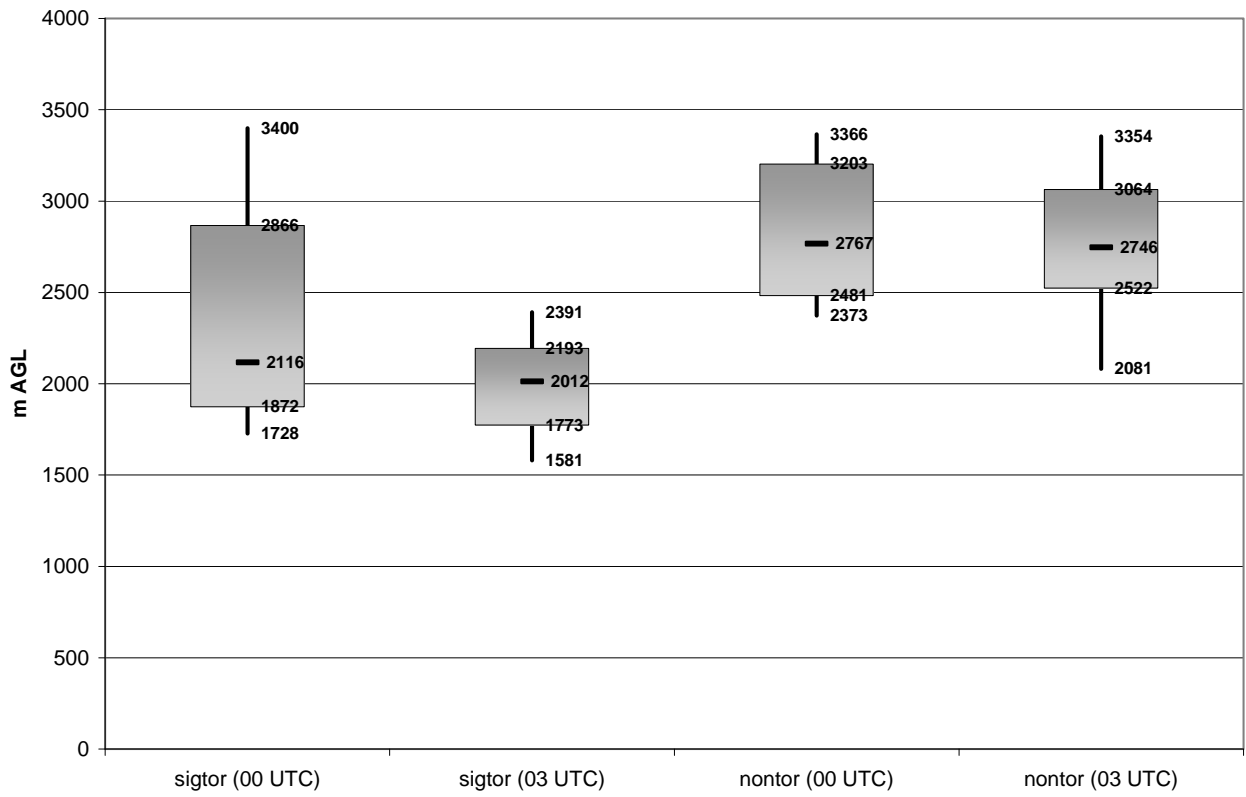


Figure 19. Same as Fig. 14, except for MLLFC (m AGL).

0-6-km VECTOR SHEAR MAGNITUDE

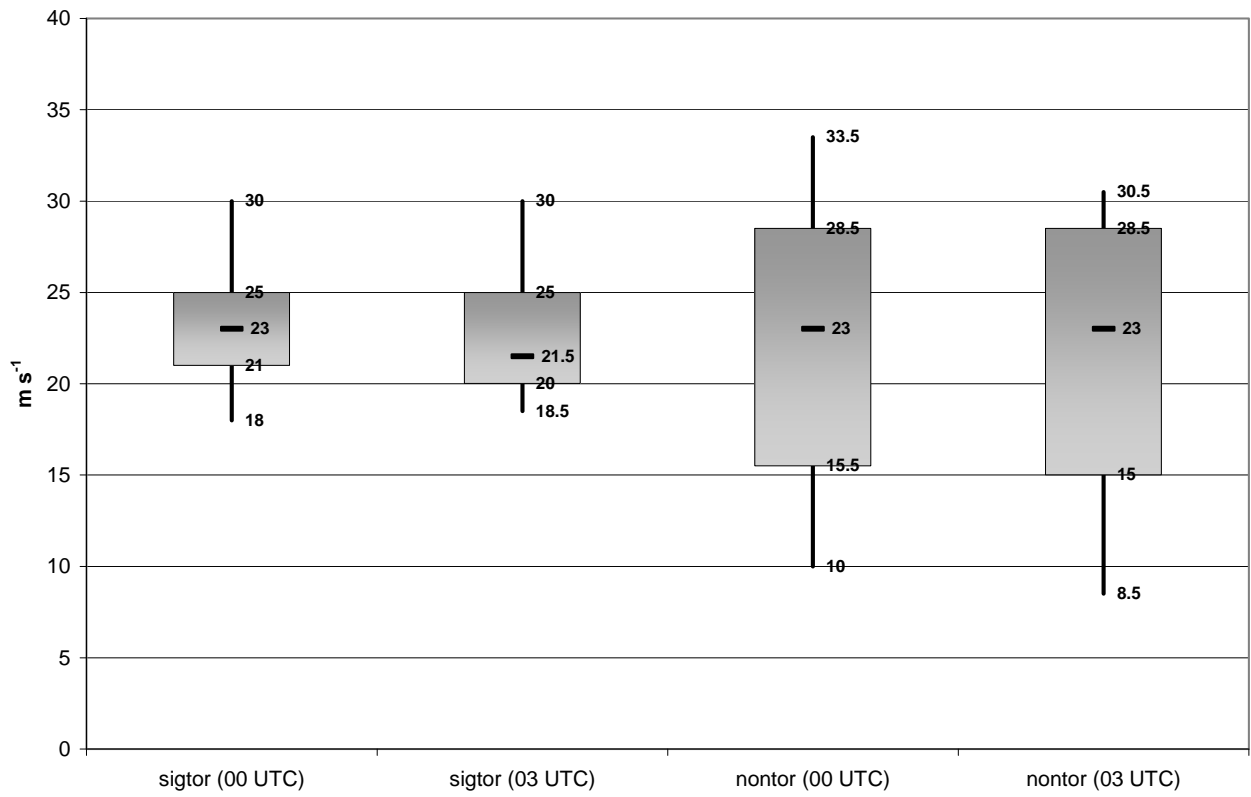


Figure 20. Same as Fig. 14, except for 0-6 km vector shear magnitude (m s^{-1}).

0-1-km SRH

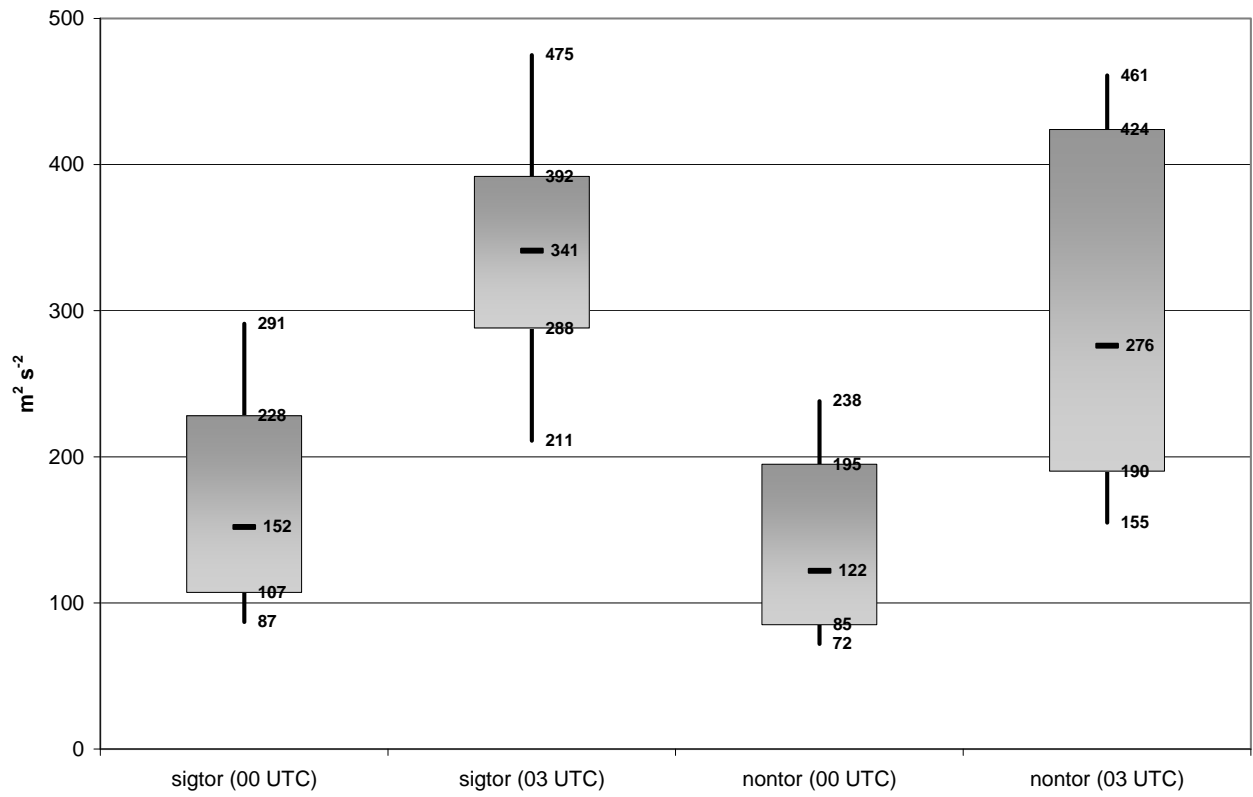


Figure 21. Same as Fig. 14, except for 0-1-km SRH ($m^2 s^{-2}$).

ESRH

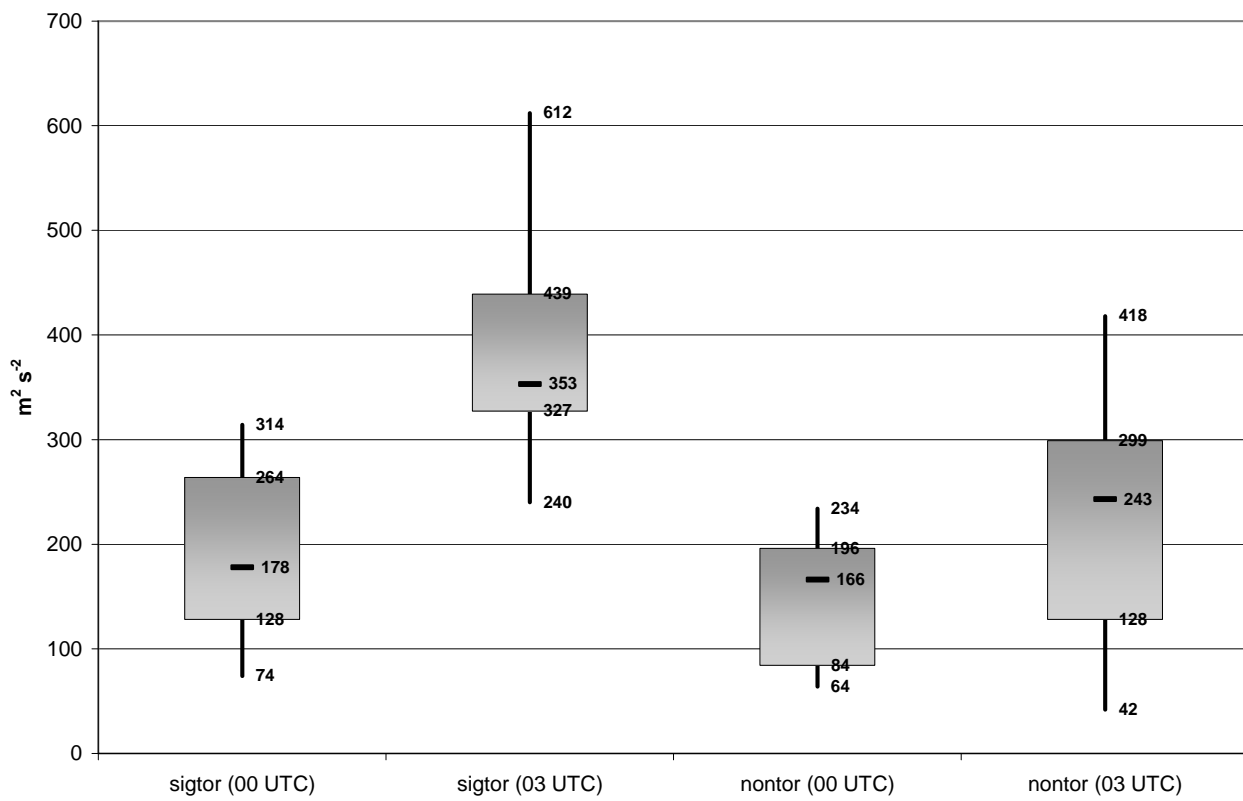


Figure 22. Same as Fig. 14, except for ESRH (m² s⁻²).

0-6-km VECTOR SHEAR MAGNITUDE

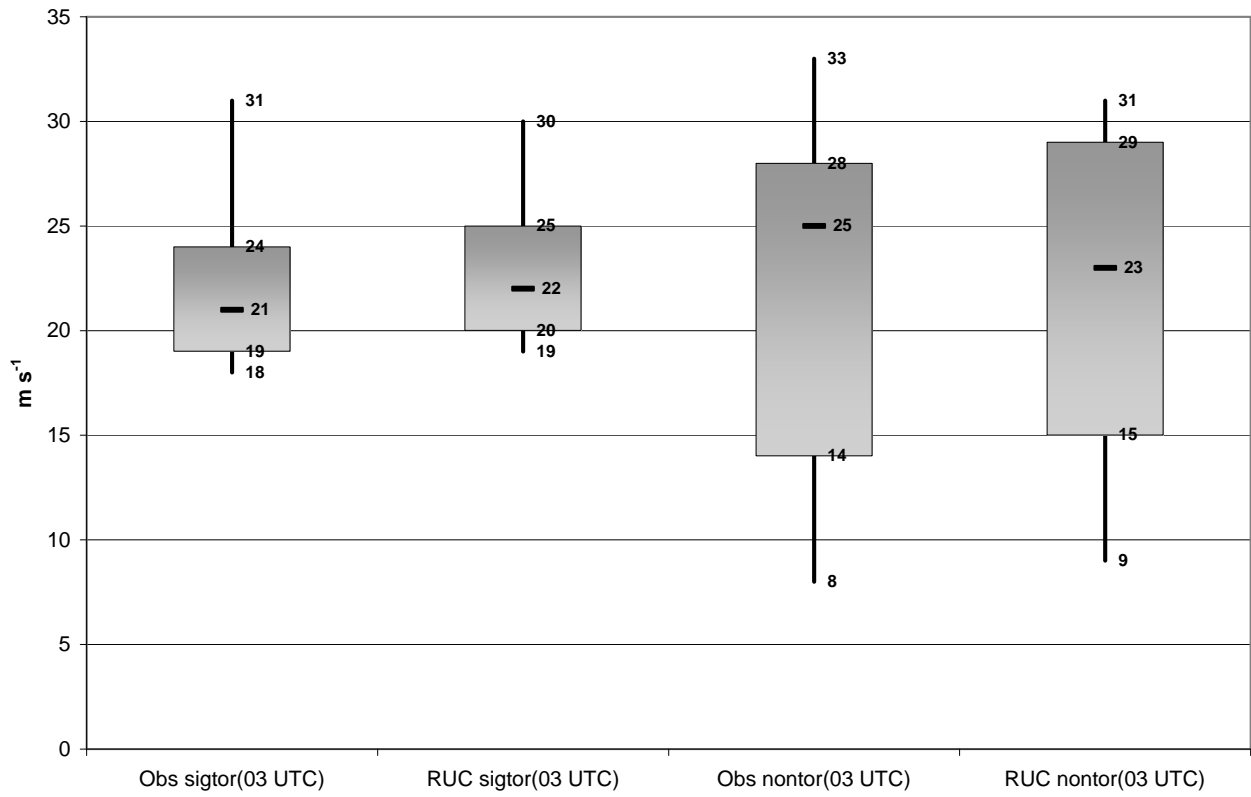


Fig. 23. 0-6-km vector shear magnitude (m s^{-1}) based on observed profiler and VAD data (conventions the same as Fig. 14).

0-1-km VECTOR SHEAR MAGNITUDE

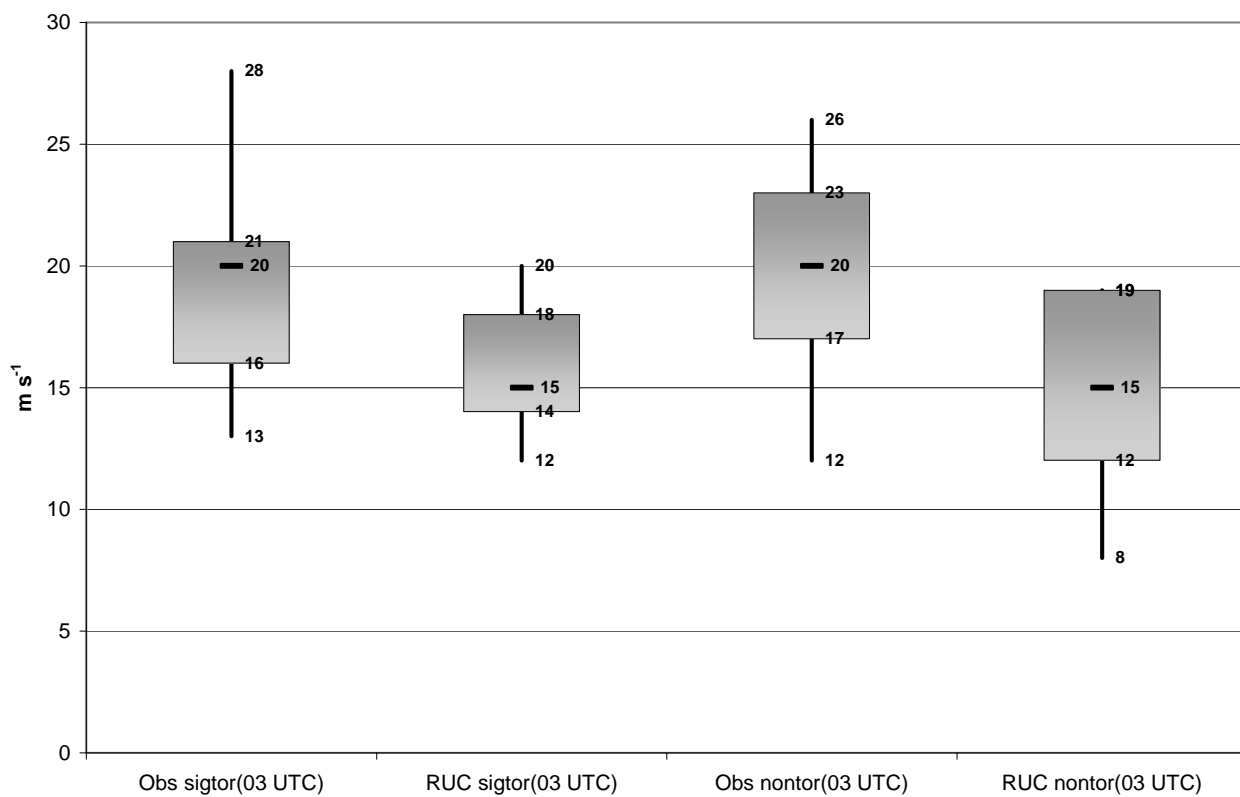


Fig. 24. Same as Fig. 23, except for 0-1-km vector shear magnitude (m s^{-1}).